www.nature.com/aps

Acta Pharmacologica Sinica

ARTICLE

Patchouli alcohol as a selective estrogen receptor β agonist ameliorates AD-like pathology of APP/PS1 model mice

Qiu-ying Yan[1], Jian-lu Lv[1], Xing-yi Shen[1], Xing-nan Ou-Yang[1], Juan-zhen Yang[1], Rui-fang Nie[1], Jian Lu[1], Yu-jie Huang[1], Jia-ying Wang[1] and Xu Shen[1]

Clinical evidence shows that postmenpausal women are almost twice as likely to develop Alzheimer's disease (AD) as men of the same age, and estrogen is closely related to the occurrence of AD. Estrogen receptor (ER) α is mainly expressed in the mammary gland and other reproductive organs like uterus while ERβ is largely distributed in the hippocampus and cardiovascular system, suggesting that ERβ selective agonist is a valuable drug against neurodegenerative diseases with low tendency in inducing cancers of breast and other reproductive organs. In this study we identified a natural product patchouli alcohol (PTA) as a selective ERβ agonist which improved the cognitive defects in female APP/PS1 mice, and explore the underlying mechanisms. Six-month-old female APP/PS1 mice were administered PTA (20, 40 mg · kg^{-1} · d^{-1}, i.g.) for 90 days. We first demonstrated that PTA bound to ERβ with a dissociation constant (K_D) of 288.9 ± 35.14 nM in microscale thermophoresis. Then we showed that PTA administration dose-dependently ameliorated cognitive defects evaluated in Morris water maze and Y-maze testes. Furthermore, PTA administration reduced amyloid plaque deposition in the hippocampus by promoting microglial phagocytosis; PTA administration improved synaptic integrity through enhancing BDNF/TrkB/CREB signaling, ameliorated oxidative stress by Catalase level, and regulated Bcl-2 family proteins in the hippocampus. The therapeutic effects of PTA were also observed in vitro: PTA (5, 10, 20 μM) dose-dependently increased phagocytosis of o-FAM-$Aβ_{42}$ in primary microglia and BV2 cells through enhancing ERβ/TLR4 signaling; PTA treatment ameliorated o-$Aβ_{25-35}$-induced reduction of synapse-related proteins VAMP2 and PSD95 in primary neurons through enhancing ERβ/BDNF/TrkB/CREB pathways; PTA treatment alleviated o-$Aβ_{25-35}$-induced oxidative stress in primary neurons through targeting ERβ and increasing Catalase expression. Together, this study has addressed the efficacy of selective ERβ agonist in the amelioration of AD and highlighted the potential of PTA as a drug lead compound against the disease.

Keywords: Alzheimer's disease; patchouli alcohol; amyloid-β; ER selective agonist; Toll-like receptor 4; synaptic plasticity

Acta Pharmacologica Sinica (2022) 43:2226–2241; https://doi.org/10.1038/s41401-021-00857-4

INTRODUCTION

Alzheimer's disease (AD) is a progressively neurodegenerative disease with progressively irreversible loss of memory and decline of intellectual and social skills [1]. The pathological hallmarks of AD include the extracellular senile plaques formed by amyloid-β (Aβ) peptide and synaptic loss [2]. Currently, there has been yet no curative medication against AD and only several drugs were approved by FDA, including cholinesterase inhibitors (e.g., tacrine, donepezil, galantamine, and rivastigmine) and a N-methyl-D-aspartate (NMDA) receptor partial antagonist (memantine), but these drugs can only improve the symptoms of AD [3]. Thus, it is much needed to design anti-AD drug based on new strategies and targets.

Epidemiologically, sex difference is tightly associated with AD development and progression. As indicated in the published reports, nearly 2/3 AD patients are female, and the risk of developing AD is higher in postmenopausal women [4]. Moreover, female AD patients show a broader spectrum of dementia-related behavioral symptoms than male [5]. Actually, estrogen plays an important role in maintenance of brain functions, including neuronal development and survival [6–8], neuroprotective [9, 10], neurotrophic [11, 12], antioxidative [13], anti-inflammatory [14], and other effects [15, 16]. It was noted that the Women's Health Initiate Memory Study approved the "critical window hypothesis" according to the results of hormone therapy suggesting that estrogen treatment may obtain the best effect on AD prevention shortly after menopause [17].

Estradiol acts targeting estrogen receptor (ER) that consists of two subtypes ERα and ERβ [18]. ERα is found mainly in the mammary gland, uterus and other reproductive organs, whereas ERβ is largely distributed in the hippocampus and cardiovascular system. Since excess activation of ERα may induce the risk of developing a series of cancers including breast cancer, endometrial cancer and ovarian cancer [19], ERβ selective agonist is believed to be capable of ameliorating cognitive impairment by avoiding the above-mentioned side effects from ERα activation [17]. Currently, ERβ selective agonists have been reported with capability in ameliorating cognitive impairment in AD model mice.

[1]Jiangsu Key Laboratory for Pharmacology and Safety Evaluation of Chinese Materia Medica and State Key Laboratory Cultivation Base for TCM Quality and Efficacy, Nanjing University of Chinese Medicine, Nanjing 210023, China
Correspondence: Jia-ying Wang (wangjy@njucm.edu.cn) or Xu Shen (xshen@njucm.edu.cn)
These authors contributed equally: Qiu-ying Yan, Jian-lu Lv

Received: 21 August 2021 Accepted: 28 December 2021
Published online: 28 January 2022

For example, genistein improved Aβ-induced cognitive impairment in rats [20], and hydroxytyrosol acetate improved the cognitive function of APP/PS1 mice [21]. Although the detailed pharmacological mechanisms are not well understood for these compounds, the published reports have clearly supported the beneficial effects of selective ERβ agonists on the amelioration of cognitive impairment of AD.

In the current work, we reported that natural product patchouli alcohol (PTA) (Fig. 1a) [22] as a selective agonist of ERβ efficiently ameliorated AD-like pathology of APP/PS1 model mice. PTA is a tricyclic sesquiterpene, and a critically biological active constituent in the patchouli oil extracted from *Pogostemon cablin* [23]. PTA exhibited varied biological activities including immunomodulation [24], anti-inflammation [25, 26], anti-tumor [27], and anti-oxidation [28]. Here, the mechanism underlying the amelioration of PTA on cognitive impairment of APP/PS1 AD model mice has been intensively investigated. PTA administration reduced Aβ deposition, enhanced synaptic plasticity and reduced oxidative stress. To our knowledge, our work might be the first to present the evidence that ERβ agonist may enhance microglial phagocytosis of o-$A\beta_{42}$ via Toll-like receptor 4 (TLR4) signaling. All results have highly addressed the beneficial effects of selective ERβ agonists on the amelioration of AD-like pathology and highlighted the potential of PTA in the treatment of AD.

MATERIALS AND METHODS

Materials

Dulbecco's modified Eagle's medium (DMEM) and DMEM-F12 cultures were obtained from Hyclone (Logan, UT, USA). Fetal bovine serum (FBS), trypsin-EDTA, glutamine and penicillin (100 U/mL)-streptomycin (100 μg/mL) (P/S) were purchased from Gibco (Gaithersburg, MD, USA). PTA was purchased from TargetMol (Shanghai, China). $A\beta_{25\text{-}35}$ was obtained from MCE (Monmouth Junction, NJ, USA). DNase, thioflavin S and poly-*D*-lysine (PDL) were obtained from Sigma-Aldrich (Sigma-Aldrich, MO, USA). FD Rapid Golgi Stain Kit was purchased from FD Neuro Technologies (Ellicott City, MD, USA). *siRNAs* were purchased from Genomeditech (Shanghai) Co., LTD (Shanghai, China). FAM-o-$A\beta_{42}$ and human $A\beta_{42}$ were obtained from ANASPEC (Fremont, CA, USA). The assay kits for BCA assay, malondialdehyde (MDA) assay, mitochondrial membrane potential (MMP) assay kit, Hoechst3442 and DEPC solution were obtained from Beyotime Biotechnology (Shanghai, China). Antibodies against vesicle-associated membrane protein (VAMP) 2, postsynaptic density (PSD) 95, tropomyosin receptor kinase B (TrkB), cAMP-response element binding protein (CREB), p-CREB (Ser133), Aβ, Bax, Bcl-xl, glial fibrillary acidic protein (GFAP), ERβ, NDUFS3 and COXIV were obtained from Cell Signaling Technology (Danvers, MA, USA). Antibodies against brain-derived neurotrophic factor (BDNF), p-TrkB (Tyr 705), and Bcl-2 were obtained from Abcam (Cambridge, UK). Antibody against ionized calcium-binding adaptor molecule 1 (Iba1) was obtained from Wako (Osaka, Japan). Antibodies against GAPDH and TLR4 were obtained from Proteintech (Chicago, IL, USA).

Luciferase reporter assay

Transactivation experiment was carried out according to the published approach [29]. Briefly, HEK293T cells were seeded at a density of 5×10^4 cells/well in 48-well plates and cultured overnight. Transient transfections (200 ng/well ERα/β, 200 ng/well pGL3-ERE-Luc and 50 ng/well pRL-SV40) were conducted by Calcium Phosphate Cell Transfection kit (Beyotime). After 6 h, HEK293T cells were incubated with PTA for 24 h. Finally, firefly and renilla luciferase activities were measured by dual luciferase reporter assay system kit (Promega, Madison, WI, USA).

Microscale thermophoresis (MST)

MST assay was performed on a Monolith NT.115 instrument (Nano Temper, Beijing, China) with Monolith His-Tag labeling kit RED-TRIS-NTA 2nd generation (MO-L018, Nano Temper, Beijing, China) according to the manufacturer's instructions. His-ERβ protein (CSB-YP007831HU, CUSABIO, Wuhan, China) was labeled with primary-amine coupling of MO-LO18 dye, followed by addition of different concentrations of PTA (0.012–400 μM). After incubation for 0.5 h, the mixtures were loaded into capillaries. Data analysis was performed with Nano Temper Analysis software.

Cell cultures

Cell line. BV2 cells were grown in DMEM/F12 (Hyclone) supplemented with 10% FBS (Gibco) and 100 unit/mL penicillin-streptomycin (Gibco), respectively.

Primary neuronal cell. The cells were prepared according to the published approach [30]. Briefly, pregnant 18-day-old C57BL/6 mice were anesthetized, and cerebral cortices were isolated from embryos and placed into cold magnesium free Hank's balance salt solution (HBSS). Cortices were cut into pieces and digested in 0.125% trypsin-EDTA with 200 U/mL DNase for 15–20 min at 37 °C in a 5% CO_2 incubator. Digestion was stopped by adding 4 mL DMEM supplemented with 10% FBS and P/S. Digested tissues were filtered through a 70 μm nylon cell strainer. Primary neurons were placed into DMEM supplemented with 10% FBS and 1% P/S, and then plated on the culture plates coated with 10 μg/mL PDL at a density of 6×10^5 cell/mL. After the plate was incubated at 37 °C in a 5% CO_2 incubator for 6 h, the medium was replaced with a fresh neurobasal medium supplemented with B27, P/S and 0.5 mM glutamine. Finally, the medium was replaced with fresh medium after 48 h, until day 7. Given that $A\beta_{25\text{-}35}$ as a toxic fragment of full-length Aβ was appropriately applied to model neuronal damage [31, 32], we here used $A\beta_{25\text{-}35}$ to induce synaptic damage and oxidative stress. $A\beta_{25\text{-}35}$ oligomers (o-$A\beta_{25\text{-}35}$) were prepared based on the published approach [32]. Cells were treated by PTA (5, 10, and 20 μM) with o-$A\beta_{25\text{-}35}$ (20 μM) for 24 h.

Primary microglia. The cells were prepared according to the published approach [33]. Briefly, cerebral cortices of C57BL/6 mice born within 24 h were isolated and placed into cold magnesium free D-Hank's balance salt solution (D-Hank's). Cortices were digested in 0.25% trypsin-EDTA with 200 U/mL DNase for 6 min, and digestion was stopped by DMEM-F12 supplemented with 10% FBS and 1% P/S. The digested tissue was blown into a suspension using a pipette and centrifuged at 1500 r/min for 15 min, and the pellets were resuspended in 10 mL DMEM-F12 and filtered through a 70 μm nylon cell strainer. The cells were transferred into cell culture flask at proper density and incubated at 37 °C with 5% CO_2. The culture flasks were shaken to remove unattached cells for 48 h. After two shakes, the cells were cultured for another week to obtain microglia.

It was noted that $A\beta_{42}$ is highly increased in the cortex and hippocampus of AD patients [34] and is a major constituent of senile plaques [35], while $A\beta_{42}$ has been applied in microglial phagocytosis assay [36]. Thus, $A\beta_{42}$ was also used in the assay to detect the effect of PTA on microglial phagocytosis. $A\beta_{42}$ oligomers (o-$A\beta_{42}$) were prepared based on the published approach [36].

Microglia were seeded into 24-well plates coated with PDL for 24 h, and then treated with 2 μg/mL o-$A\beta_{42}$ or 200 nM FAM-o-$A\beta_{42}$ and different concentrations of PTA for 4 h. Fluorescence changes were detected by using IncuCyteZoom (Ann Arbor, MI, USA) or ImageXpress Micro Confocal (Molecular Devices, LLC, Sunnyvale, CA, USA). RNA was extracted for qPCR assay.

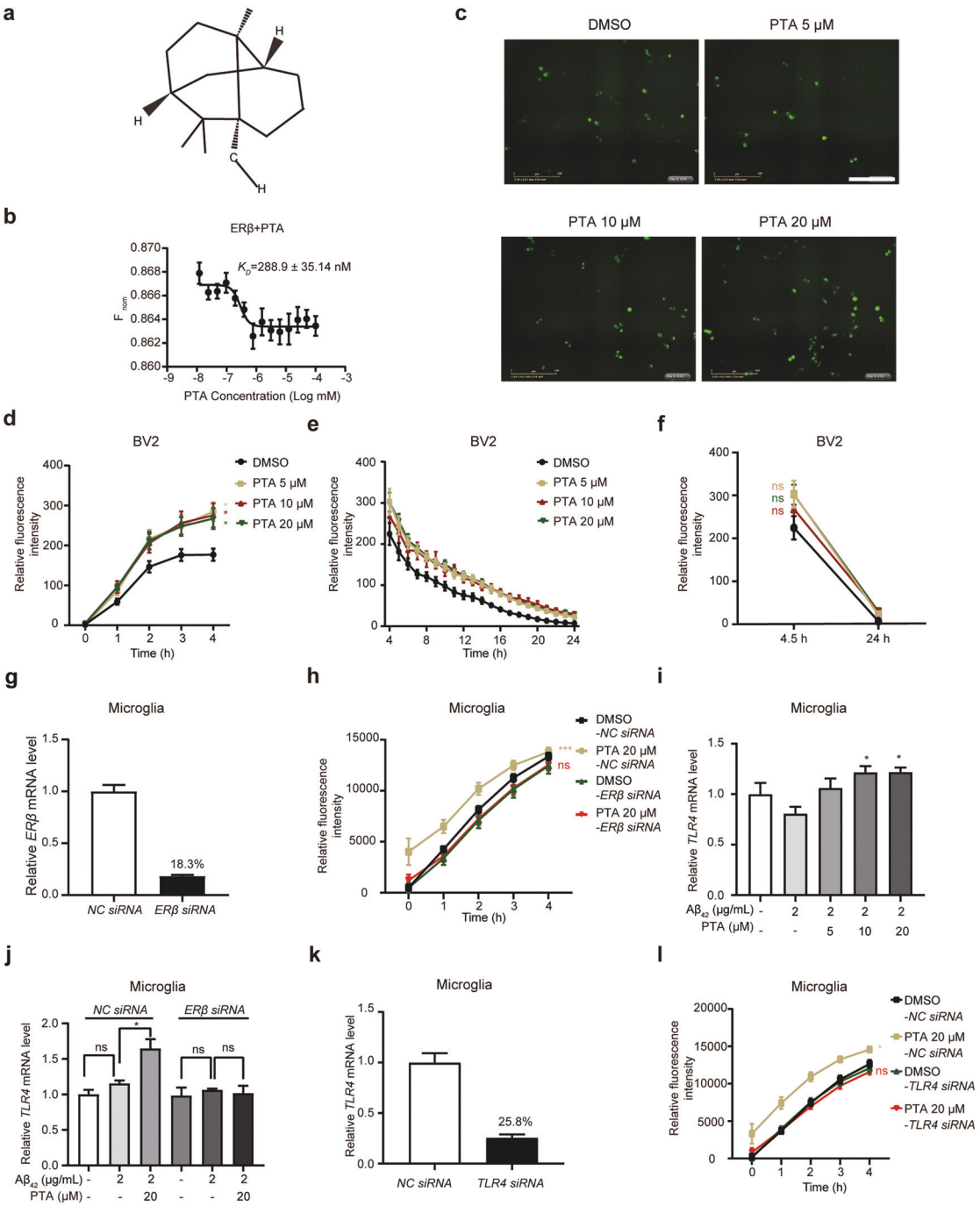

Fig. 1 PTA enhanced microglial phagocytosis of o-Aβ_{42} through ERβ/TLR4 signaling. a Chemical structure of PTA. **b** MST assay result indicated that PTA bound to ERβ by K_D at 288.9 ± 35.14 nM ($n = 4$). **c**, **d** Live cell imaging assay with quantification results demonstrated that PTA (5, 10, 20 μM) treatment increased phagocytosis of FAM-o-Aβ_{42} (200 nM) in BV2 cells. $^{***}P < 0.001$ vs DMSO group, two-way ANOVA followed by Bonferroni's multiple comparisons test. $n = 9$. Scale bar: 200 μm. Representative image at 4 h. **e**, **f** Quantification of live cell imaging assay indicated that PTA (5, 10, 20 μM) treatment had no effects on the degradation of FAM-o-Aβ_{42} (200 nM) in BV2 cells. ns represented no significant vs DMSO group, two-way ANOVA followed by Bonferroni's multiple comparisons test. $n = 9$. **g** qPCR assay results indicated that the level of ERβ mRNA in primary microglia was decreased to 18.3% after *ERβ siRNA* treatment. ($n = 3$). **h** *ERβ siRNA* deprived PTA (20 μM) of its capability in promoting FAM-o-Aβ_{42} (200 nM) phagocytosis in primary microglia. $^{***}P < 0.001$ vs DMSO-*NC siRNA*, two-way ANOVA followed by Bonferroni's multiple comparisons test. $n = 9$. qPCR assay results indicated that (**i**) PTA (5, 10, 20 μM) promoted TLR4 expression and (**j**) *ERβ siRNA* treatment deprived PTA (20 μM) of its such promotion in primary microglia. ns represented no significant, $^{*}P < 0.05$ vs Aβ-treated group, one-way ANOVA followed by Bonferroni's multiple comparisons test. $n = 3$. qPCR assay results indicated that (**k**) TLR4 level in primary microglia was decreased to 25.8% after *TLR4 siRNA* treatment ($n = 3$) and (**l**) *TLR4 siRNA* treatment deprived PTA (20 μM) of its promotion on FAM-o-Aβ_{42} (200 nM) phagocytosis in primary microglia. $^{*}P < 0.05$ vs DMSO-*NC siRNA*, ns represented no significant vs DMSO-*TLR4 siRNA*, two-way ANOVA followed by Bonferroni's multiple comparisons test. $n = 9$.

Cell transfection with *siRNA*

ERβ siRNA and *TLR4 siRNA* were purchased from Genomeditech (Shanghai) Co., Ltd (Shanghai, China). The target sequence in mouse ERβ for *siRNA* oligonucleotide duplexes was 5′-GGUCC-CAUCUAUAUCCCUU-3′, the target sequence in mouse TLR4 for *siRNA* oligonucleotide duplexes was 5′-GCAUAGAGGUAGUUC-CUAAUA-3′.

Primary neurons or microglia were seeded into culture plate and cultured for 24 h, and then treated with *negative control* (*NC*) or *ERβ siRNA* or *TLR4 siRNA* by using Lipofectamine 2000 and incubated for 6 h at 37 °C. ERβ or TLR4 silencing efficacy of *siRNA* was evaluated by qPCR 48 h or 24 h later (Fig. 1g, k, and Supplementary Fig. S2a).

Mitochondrial membrane potential (MMP) assay

MMP level was detected according to the manufacturer's instructions. Briefly, the cells cultured in plates were aspirated and washed once with PBS buffer. JC-1 staining working solution was added in the plate and incubated at 37 °C for 20 min. The supernatant was then removed, and cells were washed twice with JC-1 staining buffer (1×). Pictures were taken by using Lecia DMI8 microscope (Lecia, Germany) and subsequently analyzed by ImageJ software system (NIH Image, Bethesda, MD, USA). Finally, MMP level was calculated by red fluorescence intensity/green fluorescence intensity.

CUT&Tag assay

CUT&Tag assay was performed by Hieff NGS® G-Type In-Situ DNA Binding Profiling Library Prep Kit for Illumina (Cat No. 12598, Yeasen Biotechnology, Shanghai, China) according to the manufacturer's instructions. Briefly, primary neurons or microglia were harvested, washed, and collected. To the cells were added activated paramagnetic Concanavalin A beads, followed by incubation with primary or secondary antibody at room temperature (RT). Cells were washed twice with magnet stand to remove unbound antibodies and incubated with 1 μL pA/G-Transposome Mix for 1 h at RT. Next, cells were resuspended in Tagmentation Buffer and incubated at 37 °C for 1 h. Then, 2 μL 15× Terminate Solution, 1 μL DNA Spike-in mix and 1 μL 30× Proteinase K were added to 31 μL of sample, followed by incubation at 55 °C for 30 min.

To amplify libraries, 20 μL DNA was mixed with 3 μL PCR Primer Mix, 1 μL N502, 1 μL N701 and 25 μL 2× Ultima Amplification Mix. Then, samples were placed in a Thermocycler with a heated lid using the following cycling conditions: 72 °C for 3 min; 95 °C for 30 s; 15 cycles of 95 °C for 10 s, 55 °C for 30 s and 72 °C for 30 s; final extension at 72 °C for 5 min and hold at 4 °C. Post-PCR clean-up was performed by adding 1.2× volume of DNA Selection Beads, and libraries were incubated with beads at RT for 5 min, washed twice gently in 80% ethanol, and eluted in 21 μL ddH_2O.

Animals

All animal experiments were performed in accordance with the institutional ethical guidelines on animal care of Nanjing University of Chinese Medicine.

B6SJL-transgenic (APP/PS1) female mice (6 month) were purchased from GemPharmatech (Nanjing, China). Each mouse was housed in each cage and maintained in a temperature controlled (22 ± 2 °C) environment and humidity (45% ± 10%) for 12 h in the light and 12 h in dark cycle during the experiment period. Mice were allowed to freely access to food and water. The study protocol was approved by the Ethics Committee of Nanjing University of Chinese Medicine.

Animal group and PTA administration

After acclimatization for 7 days, thirty-six of 6-month-old female APP/PS1 mice were randomly divided into three groups and twelve 6-month-old wild-type (WT) mice were used as a NC. PTA was dissolved in saline solution containing 2% (*v/v*) DMSO and 1% (*v/v*) Tween 80. Three groups of female APP/PS1 mice were administered 20, 40 $mg \cdot kg^{-1} \cdot d^{-1}$ PTA and vehicle (saline solution containing 2% (*v/v*) DMSO and 1% (*v/v*) Tween 80), and WT group of mice was administered vehicle by oral gavage for 90 days. After 90-day treatment with PTA, Morris water maze (MWM) and Y-maze were applied to evaluate the cognitive ability and spatial working memory of mice.

Behavioral experiment

Morris water maze test. Morris water maze (MWM) was performed according to the published method [37]. Briefly, during over 7 consecutive days with three trials per day, mice were trained to use a variety of visual cues located on the pool wall to find a hidden submerged white platform in a circular pool (120 cm in diameter, 50 cm deep) filled with white-tinted water. For each training day, mouse was placed in the water facing the pool wall from three different positions to find the hidden platform within 90 s. If the mouse found the platform, it was allowed to stay on it for 15 s. If the mouse failed to find the platform within 90 s, the animal was guided to the platform and kept there for 15 s. On the 8th day, the platform was removed to test memory retention of the mice. The mice were allowed to swim for 90 s in search for it. All data were collected for mouse performance analysis. For data analysis, the pool was divided into four equal quadrants formed by imaging lines, and intersected in the center of the pool at right angles called north, south, east, and west.

Y-maze test. The test was performed according to the published methods [38]. The mice were placed in the maze with the same starting arm, and allowed to explore freely on the three arms for 5 min. A mouse entering three different arms was continuously recorded as a completing spontaneous alternation. The maximum spontaneous alternation is the sum of the number of arms advances - 2. Percentage of spontaneous alternation reaction = actually completed spontaneous alternation/the maximum spontaneous alternation × 100%. All movements were recorded through a video camera and the percentage of correct alteration was calculated.

Brain sample processing

After behavioral assays, mice were euthanized, and brains were removed rapidly and bisected in a mid-sagittal plane. The right hemisphere was divided into cortex and hippocampus and stored at −80 °C for further analysis. The left hemispheres were fixed with 4% paraformaldehyde for 24 h, and then cryoprotected in phosphate-buffered saline (PBS) containing 30% sucrose. The tissue was embedded in OCT and cut in the coronal plane into 20 μm slices for further pathological and immunofluorescence assays. In addition, the whole brains of three mice in each group were used for Golgi staining experiment by using a Rapid Golgi Stain Kit.

Microglial phagocytosis of o-$A\beta_{42}$

Cell-based assay. $A\beta_{42}$ oligomers were prepared based on the published approach [39]. In o-$A\beta_{42}$ phagocytosis assay, BV2 cells or primary microglia were incubated with FAM-o-$A\beta_{42}$ (200 nM) and PTA for 4 h. IncuCyte Zoom detector was used for recording FAM-o-$A\beta_{42}$ phagocytosis process. In the assay, at least 5000 cells from each group were analyzed from three independent experiments.

Tissue-based assay. Given that Iba1 is a calcium-binding protein that expresses specifically in microglia of the brain [40], Iba1 antibody was used to label microglia in the assay for investigating the activity of PTA in promoting microglial phagocytosis of Aβ in APP/PS1 mice. Iba1/Aβ colocalization percentage was measured by the "colocalization rate" in the ImageJ software.

Table. 1. Primer sequences.

Primers		Primer sequences (5′ to 3′)
BDNF	Forward	AGCCTCCTCTGCTCTTTCTGCTGGA
	Reverse	CTTTTGTCTATGCCCCTGCAGCCTT
Catalase	Forward	GCAGATACCTGTGAACTGTC
	Reverse	GTAGAATGTCCGCACCTGAG
ERβ	Forward	CTGTGATGAACTACAGTGTTCCC
	Reverse	CACATTTGGGCTTGCAGTCTG
GAPDH	Forward	ACAGCAACAGGGTGGTGGAC
	Reverse	TTTGAGGGTGCAGCGAACTT
TLR4	Forward	ATGGCATGGCTTACACCACC
	Reverse	GAGGCCAATTTTGTCTCCACA

Western blot
Primary neurons and brain tissue were lysed in RIPA buffer (Beyotime) containing a protease and phosphorylase inhibitor cocktails (Thermo Scientific, Cleveland, OH, USA) on ice. Protein concentration was determined by using BCA protein assay kit (Beyotime). Equal amounts of protein from each sample were separated in SDS-PAGE gels, proteins were transferred to a polyvinylidene difluoride membrane (Immobilon) by electrophoresis apparatus. After blocking nonspecific binding in 5% skimmed milk for 2 h at RT, the membranes were incubated with primary antibodies (dilution 1:1000) overnight at 4 °C and washed, followed by incubation with secondary antibody (dilution 1:3000) conjugated with horseradish peroxidase (Jackson ImmunoResearch, Cambridge, UK) reaction for 2 h at RT. Immunoreactive bands were visualized and enhanced by the Dura detection system (Thermo Scientific). The density of protein brands was quantified using ImageJ software.

Quantitative real-time PCR
Total RNA from cells or tissues was isolated with RNAiso plus reagent according to the manufacture's protocol. cDNA synthesis was performed with oligo-dT as the primer using reverse-PCR kit (TaKaRa Biotechnology, Dalian, China). qPCR was performed on Bio-Rad real-time PRC detection system with SYBR Premix Ex Taq kit. Relative transcript levels were calculated by $2^{-\Delta\Delta Ct}$ method [41].

Primer sequences for analysis of BDNF, Catalase, ERβ, GAPDH, and TLR4 mRNA were shown in Table 1.

The brain tissues of four mice in each group were selected for qPCR detection.

Immunostaining assay
Primary neuron cell-based assay. After incubation of o-$A\beta_{25-35}$ (20 μM) with different concentrations of PTA for 24 h, the extracellular medium was washed away three times using PBS buffer (pH 7.4), followed by postfix in 4% PFA for 25 min at RT. The cells were blocked against nonspecific binding in 4% BSA for 30 min at RT and incubated overnight at 4 °C with primary antibody (dilution 1:250). Then, the slides were washed with PBS three times and incubated with secondary antibody (dilution 1:1000) for 30 min at RT. Finally, samples were incubated with Hoechst 33342 solution for 3–5 min, and detected by a fluorescence microscope (Leica, Germany). The images were analyzed by the ImageJ software.

Brain tissue. Brain sections were permeabilized in PBS containing 0.3% Triton X-100, then blocked with PBS with 4% albumin from bovine serum (BSA). The sections placed in a wet box were exposed to primary antibody overnight at 4 °C. Sections were washed with PBS and incubated with secondary antibody for 1 h at RT in dark. Finally, the sections were incubated with Hoechst 33342 solution for 3–5 min, and observed by using Leica DMI8 microscope system (Leica). The images were analyzed by the ImageJ software.

Golgi staining
The morphology of dendritic spines in the brain was analyzed using an FD Rapid Golgi Stain Kit (FD Neuro technologies, Elliot City, MD, USA) according to the manufacturer's instructions. Briefly, the whole brains were immersed in an impregnation solution consisting of solution A and B (1:1) for 2 weeks at RT in dark and subsequently transferred to solution C in dark for 3 days. The brains were then embedded using OCT (SAKURA, Finetek, CA, USA) and cut into 100 μm-thick sections by using a vibratome (Leica) and placed onto microscope slides. After drying at RT, the sections were washed twice by double-distilled water for 4 min, and then placed into a working solution composed of solution D, solution E and double-distilled water (*v*:*v*:*v*, 1:1:2) for 10 min. After washing with ddH_2O twice, the sections were dehydrated in graded alcohol solutions (50%, 75%, 95% and 100%), cleaned in xylene and covered lipped. Images of neurons were obtained by an automated upright microscope (Leica).

Thioflavin-S staining
Thioflavin-S is a fluorescent dye that specifically binds to amyloid fibrils [42]. In the assay, the brain sections were rinsed three times with 0.01 M PBS for 5 min, and incubated with 0.3% thioflavin-S (thioflavin-S in 50% alcohol) for 8 min at RT in dark. Then, the slices were washed with 50% alcohol three times for 5 min and subsequently washed with distilled water for 5 min. The images were processed using Leica DMI8 microscope, and the numbers and percentages of thioflavin-S-labeled Aβ plaques in the cortex or hippocampus were quantified by the ImageJ software system.

Malondialdehyde (MDA) assay
Detection of MDA content was performed according to the manufacturer's instructions. Briefly, the brain tissue was homogenized on ice with Western lysate buffer and centrifuged at $12000 \times g$ for 10 min. The supernatant was then taken for MDA determination. BCA assay kit was used to determine the protein concentration of the samples.

Statistical analysis
All experiments were performed in triplicate to independently obtain three experimental data. All values were expressed as mean ± standard error of the mean (SEM). Differences between two groups were analyzed with Student's *t* test, differences in the escape latency in the MWM test were analyzed using two-way ANOVA followed by Bonferroni's multiple comparisons test. And the other data were analyzed by one-way ANOVA followed by Bonferroni's multiple comparisons test. $P < 0.05$ being considered significantly. The data were analyzed for statistical significance using the graphing program GraphPad Prism 8 (San Diego, CA, USA).

RESULTS

PTA was a selective ERβ agonist
PTA was ever reported to be a selective ERβ agonist [22], but lack of detailed supporting data. Here, luciferase reporter assay was performed to verify the selective agonistic effects of PTA on the transcriptional activities of ERβ and ERα. As shown in Supplementary Fig. S1a, b, PTA agonized ERβ transcriptional activity but antagonized ERα transcriptional activity.

In addition, MST assay [43] was also performed to investigate PTA binding to ERβ. As shown in Fig. 1b, the results demonstrated that PTA bound to ERβ by dissociation constant (K_D) at 288.9 ± 35.14 nM. Moreover, immunofluorescence assay results further

indicated that PTA increased the nuclear localization of ERβ (Supplementary Fig. S1c–f).

Thus, all results verified that PTA is a selective ERβ agonist.

PTA promoted microglial phagocytosis of o-$A\beta_{42}$

PTA promoted microglial phagocytosis of o-$A\beta_{42}$ by targeting ERβ. According to the published reports, Aβ accumulation and its formed senile plaque are important pathological features of AD [44] and microglia internalize and degrade Aβ to maintain the stability of Aβ [45], while estrogen as an ERβ agonist enhanced Aβ uptake and internalization in cultured microglia [46].

With these facts, we detected the potential of PTA in promoting phagocytic and degradation abilities of BV2 cells against $A\beta_{42}$ by detecting FAM-labeled o-$A\beta_{42}$ in the cells [36]. The results demonstrated that PTA promoted the phagocytic activity of BV2 cell against FAM-o-$A\beta_{42}$ (Fig. 1c, d).

In the assay to evaluate the effect of PTA on Aβ degradation, the medium of BV2 cell was replaced by FAM-o-$A\beta_{42}$-free medium after the incubation of BV2 cell with FAM-o-$A\beta_{42}$ for 4 h. As indicated in Fig. 1e, f, PTA had no effects on Aβ degradation.

Next, *ERβ siRNA* assay was performed in primary microglia (Fig. 1h), and the results demonstrated that *ERβ siRNA* deprived PTA of its capability in promoting microglial phagocytosis of o-$A\beta_{42}$ (Fig. 1h).

Thus, all results demonstrated that PTA enhanced microglial phagocytosis of o-$A\beta_{42}$ by targeting ERβ.

PTA enhanced microglia phagocytosis of o-$A\beta_{42}$ through ERβ/TLR4 signaling. Given that TLR4 mediates $A\beta_{42}$ phagocytosis [47], we next investigated whether TLR4 signaling was responsible for the PTA-promoted $A\beta_{42}$ phagocytosis in primary microglia.

As indicated in Fig. 1i, PTA treatment increased the mRNA level of TLR4 in primary microglia, and such a PTA-induced increase was blocked by *ERβ siRNA* (Fig. 1j). This result thus demonstrated that PTA stimulated TLR4 by targeting ERβ in primary microglia.

Moreover, the results in Fig. 1k, l indicated that *TLR4 siRNA* deprived PTA of its ability in promoting FAM-o-$A\beta_{42}$ phagocytosis in primary microglia, thus demonstrating that TLR4 was required for the enhancement of PTA on microglial phagocytosis of o-$A\beta_{42}$.

Together, all results indicated that PTA enhanced microglial phagocytosis of o-$A\beta_{42}$ through ERβ/TLR4 signaling.

PTA protected synaptic integrity through ERβ/BDNF/TrkB/CREB pathway in primary neurons

PTA protected synaptic integrity by targeting ERβ. Considering that synaptic damage contributes largely to cognitive impairment [48], immunofluorescence assay was next performed to evaluate the potential of PTA in protecting synaptic integrity by detecting the expression of synaptic integrity related proteins VAMP2 and PSD95 [48–50] in primary neurons.

Immunofluorescence and Western blot assays revealed that o-$A\beta_{25-35}$ treatment suppressed the expressions of VAMP2 and PSD95, and PTA antagonized such o-$A\beta_{25-35}$-induced suppressions (Fig. 2a–f). Moreover, *ERβ siRNA* downregulated the levels of these two proteins, and deprived PTA of its above-mentioned antagonistic activity against these two proteins (Fig. 2g–l).

Therefore, all results suggested that PTA protected synaptic integrity by targeting ERβ.

PTA ameliorated o-$A\beta_{25-35}$-induced synaptic damage through ERβ/BDNF/TrkB/CREB pathway. According to the published reports, ERβ activation promoted the growth and stability of new dendritic spines and ameliorated synaptic plasticity damage in female mice [51, 52]. In addition, BDNF is an important neurotrophic factor that highly binds to TrkB, and BDNF activates the transcription factor CREB that can regulate the expression of the genes encoding the proteins related to neural plasticity [53], while ERβ regulates BDNF expression in mice [11, 54]. With these facts, we investigated the potential of PTA in regulating BDNF/TrkB/CREB signaling in primary neurons. PCR and Western blot results demonstrated that o-$A\beta_{25-35}$ suppressed mRNA and protein levels of BDNF, p-TrkB (Tyr 705) and p-CREB (Ser133), and PTA antagonized such o-$A\beta_{25-35}$-induced suppressions (Fig. 3a–e).

Notably, *ERβ siRNA* rendered no impacts on the protein level of BDNF, p-TrkB (Tyr 705) or p-CREB (Ser133), but indeed abolished the upregulation of PTA against BDNF/TrkB/CREB pathway in primary neurons (Fig. 3f–j). These results thus verified that PTA regulated BDNF/TrkB/CREB pathway by targeting ERβ, although there are varied factors regulating BDNF, TrkB, or CREB.

Thus, all results indicated that PTA ameliorated Aβ-induced synaptic damage through ERβ/BDNF/TrkB/CREB pathway.

PTA improved o-$A\beta_{25-35}$-induced mitochondrial dysfunction and oxidative stress in primary neurons

PTA ameliorated o-$A\beta_{25-35}$-induced mitochondrial damage by targeting ERβ. Given that mitochondrial dysfunction occurs in the early stage of AD with exacerbation of oxidative stress [55–57], and NDUFS3 as a core subunit of mitochondrial complex I plays a key role in electron transport of the oxidized respiratory chain [58], we investigated the potential of PTA in antagonizing the Aβ-induced mitochondrial damage in primary neurons.

MMP assay kit with JC-1 was used to detect MMP level of neurons [59]. As expected, PTA antagonized the o-$A\beta_{25-35}$-induced decrease of MMP level (Fig. 4a, b). Moreover, *ERβ siRNA* deprived PTA of its capability in antagonizing the o-$A\beta_{25-35}$ induced MMP decline (Fig. 4f, g). Western blot assay results demonstrated that PTA antagonized the o-$A\beta_{25-35}$-induced suppression of NDUFS3 (Fig. 4c, d) and *ERβ siRNA* deprived PTA of such an antagonistic capability (Fig. 4h, i) in primary neurons.

Together, all results demonstrated that PTA ameliorated mitochondrial damage in primary neurons by targeting ERβ in primary neurons.

PTA ameliorated o-$A\beta_{25-35}$-induced oxidative stress in neurons through ERβ/Catalase pathway without influence on mitochondrial ERβ protein expression. To investigate the capability of PTA in alleviating oxidative stress, the gene expression of antioxidant enzymes Catalase [60] was detected by qPCR in primary neurons. PCR results indicated that o-$A\beta_{25-35}$ inhibited Catalase expression, and PTA efficiently antagonized such o-$A\beta_{25-35}$-induced inhibition of Catalase expression in primary neurons (Fig. 4e). Meanwhile, *ERβ siRNA* treatment blocked PTA of its above-mentioned antagonistic capability (Fig. 4j).

According to the published report [61], ERβ localizes to nuclear, plasma membrane and mitochondria, and mitochondrial ERβ (mtERβ) directly affects neuronal mitochondrial function. Thus, Western blot assay was performed to evaluate the potential effect of PTA on the expression of mtERβ, and the results indicated that PTA failed to antagonize the o-$A\beta_{25-35}$-induced the decline in mtERβ protein level (Supplementary Fig. S2b, c).

Taken together, our results demonstrated that PTA alleviated oxidative stress in neurons via ERβ/Catalase pathway without influence on the protein expression of mtERβ.

ERβ bound to the promotor of BDNF but had no binding affinity to Catalase or TLR4. It was reported that ERβ regulates downstream genes through two patterns. One is that ERβ directly binds to the promotor of downstream genes, and the other is that ERβ regulates the transcriptions of downstream genes through transcription factors [19]. With these facts, CUT&Tag assay [62] was performed to investigate the potential of ERβ binding to the promoter(s) of the target gene(s).

As shown in Supplementary Fig. S6, qPCR results indicated that compared to IgG group, the level of BDNF expression was highly increased and the level of Catalase or TLR4 was almost unchanged in ERβ group. These results thus implied that ERβ bound to the

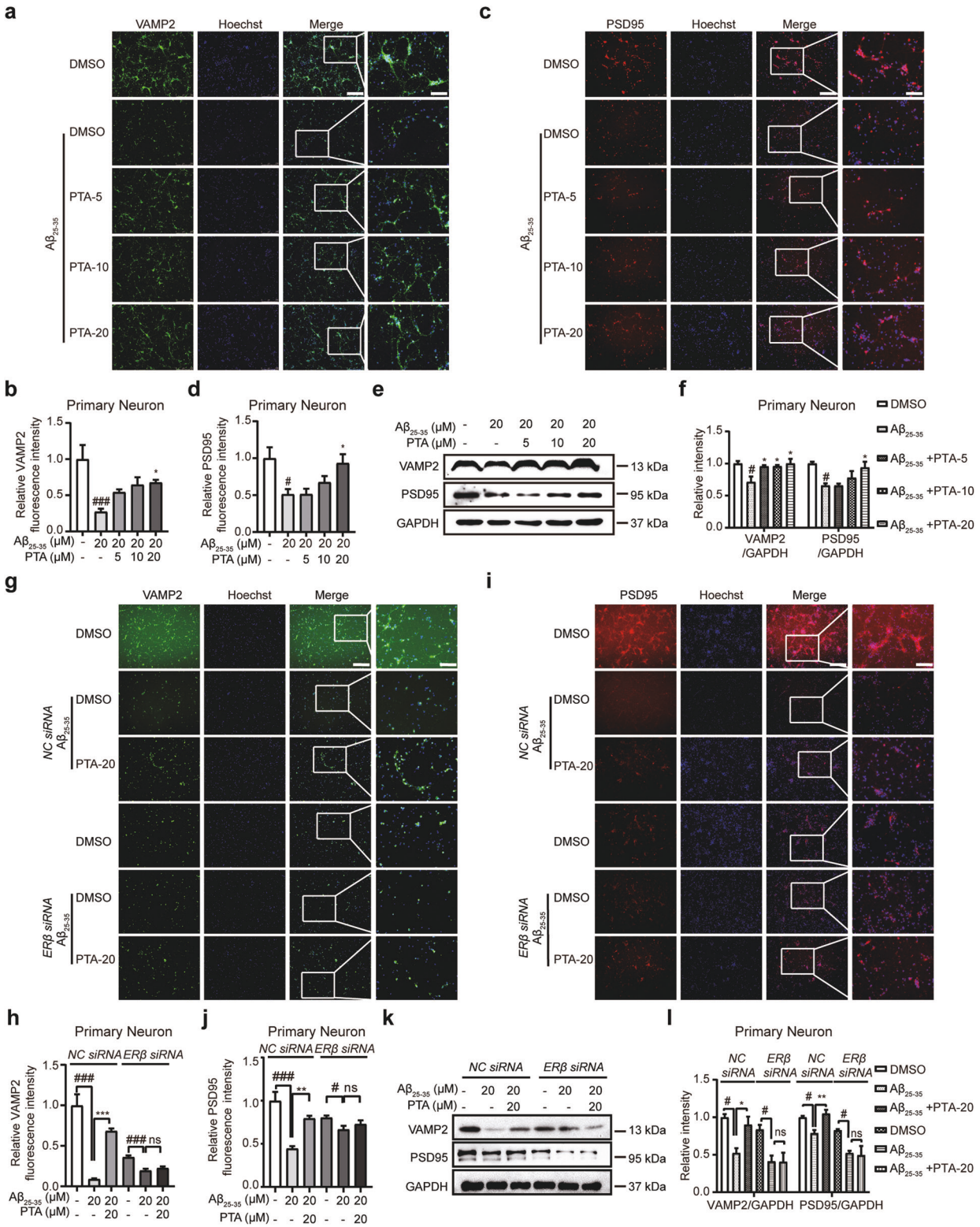

Fig. 2 PTA antagonized the o-Aβ$_{25-35}$-induced decrease in the levels of VAMP2 and PSD95 in primary neurons. a–f Immunofluorescence and Western blot assays with quantification results demonstrated that PTA (5, 10, 20 μM) antagonized the o-Aβ$_{25-35}$ (20 μM)-decreased levels of (**a**, **b**, **e**, **f**) VAMP2 and (**c**, **d**, **e**, **f**) PSD95. **g–l** Immunofluorescence and Western blot results with quantification results demonstrated that *ERβ siRNA* deprived PTA (20 μM) of its above-mentioned antagonistic activities against (**g**, **h**, **k**, **l**) VAMP2 and (**i**, **j**, **k**, **l**) PSD95. All assays were performed in primary neurons. $^{\#}P < 0.05$ and $^{\#\#\#}P < 0.001$ vs DMSO, $^{*}P < 0.05$, $^{**}P < 0.01$, $^{***}P < 0.001$ vs o-Aβ$_{25-35}$, one-way ANOVA followed by Bonferroni's multiple comparisons test. $n \geq 3$. Scale bar: 250 μm, 100 μm.

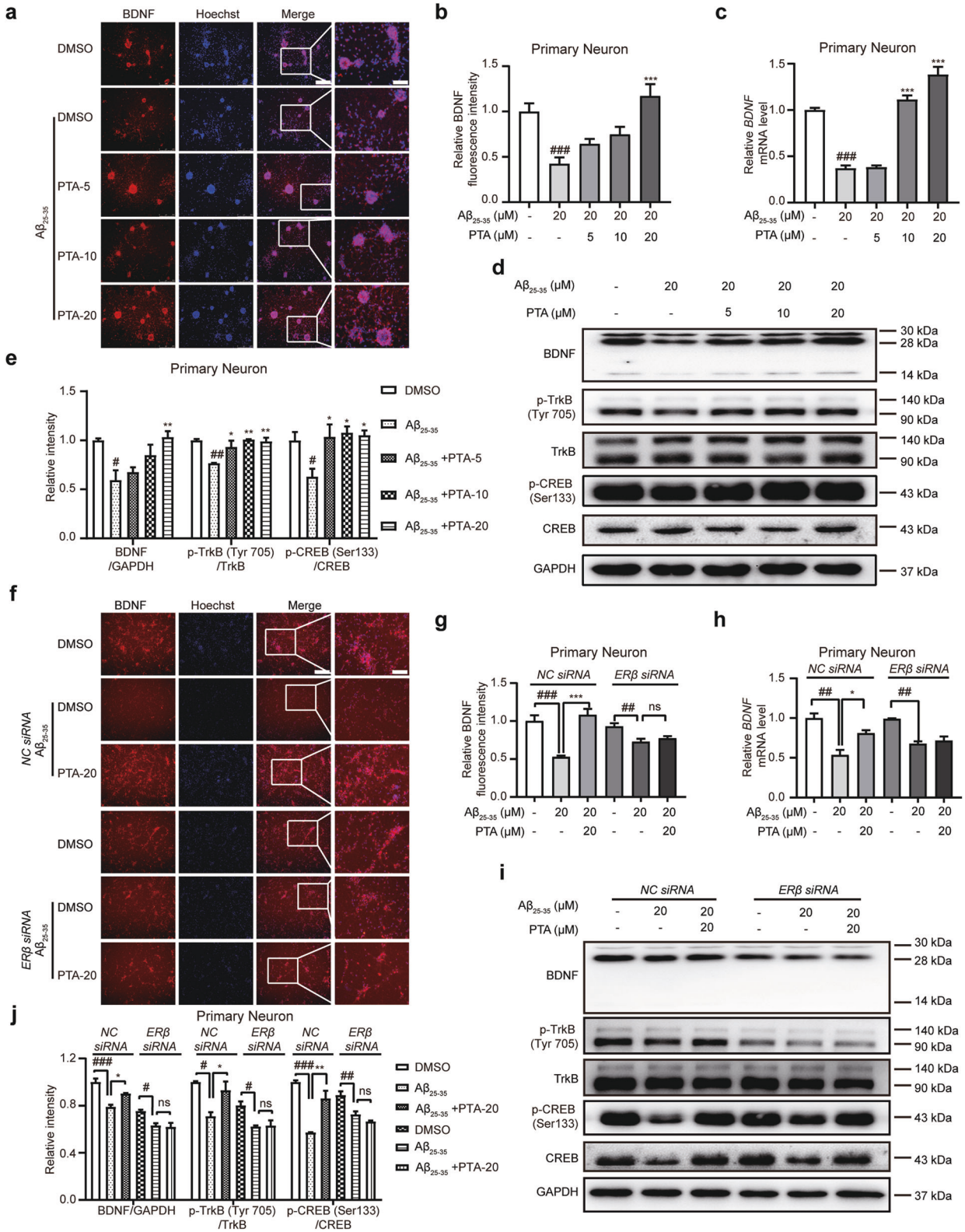

Fig. 3 PTA antagonized o-Aβ$_{25-35}$-induced suppression on ERβ/BDNF/TrkB/CREB pathway in primary neurons. a, **b** Immunofluorescence and (**c**) qPCR assay results indicated that PTA (5, 10, 20 μM) reversed the o-Aβ$_{25-35}$ (20 μM) -induced decrease of BDNF ($n \geq 3$). **d**, **e** Western blot with quantification results showed that PTA (5, 10, 20 μM) antagonized the o-Aβ$_{25-35}$ (20 μM)-induced decrease in protein levels of BDNF, p-TrkB (Tyr 705), p-CREB (Ser133) ($n = 3$). **f**, **g** Immunofluorescence and (**h**) qPCR assays results demonstrated that *ERβ siRNA* deprived PTA (20 μM) of its capability in antagonizing the o-Aβ$_{25-35}$ (20 μM)-induced decrease of BDNF. **i**, **j** Western blot assay with qualification indicated that *ERβ siRNA* deprived PTA (20 μM) of its antagonistic capability against o-Aβ$_{25-35}$ (20 μM)-induced suppression on the protein expression levels of BDNF, p-TrkB (Tyr 705), p-CREB (Ser133). All assays were performed in primary neurons. $^{\#}P < 0.05$, $^{\#\#}P < 0.01$ and $^{\#\#\#}P < 0.001$ vs DMSO, $^{*}P < 0.05$, $^{**}P < 0.01$ and $^{***}P < 0.001$ vs o-Aβ$_{25-35}$, ns represented no significant, one-way ANOVA followed by Bonferroni's multiple comparisons test. $n \geq 3$. Scale bar: 250 μm, 100 μm.

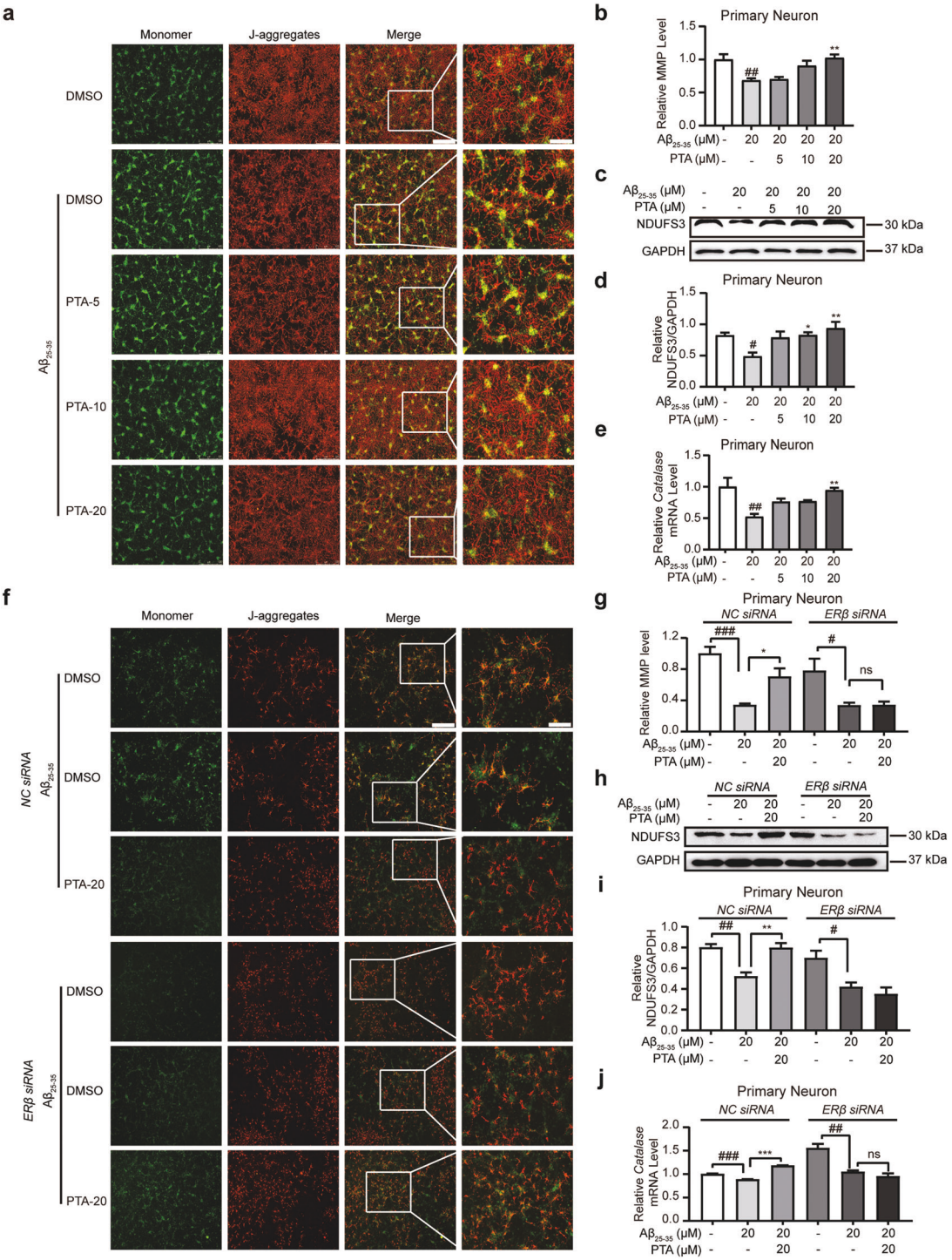

Fig. 4 PTA improved o-Aβ$_{25-35}$-induced mitochondrial dysfunction and Catalase expression decrease by targeting ERβ in primary neurons. a, **b** Immunofluorescence assay with quantification results indicated that PTA (5, 10, 20 μM) antagonized the o-Aβ$_{25-35}$ (20 μM)-induced MMP decline ($n = 5$). **c**, **d** Western blot assay with quantification results demonstrated that PTA (5, 10, 20 μM) antagonized the o-Aβ$_{25-35}$ (20 μM)-induced decline in NDUFS3 protein level ($n = 3$). **e** qPCR assay result demonstrated that PTA (5, 10, 20 μM) antagonized the o-Aβ$_{25-35}$ (20 μM)-induced decrease in Catalase expression ($n = 3$). **f**, **g** Immunofluorescence and quantification results demonstrated that PTA (5, 10, 20 μM) reversed the o-Aβ$_{25-35}$ (20 μM)-induced decrease in MMP by targeting ERβ ($n = 5$). **h**, **i** Western blot assay with quantification results demonstrated that *ERβ siRNA* deprived PTA (20 μM) of its capability in antagonizing the o-Aβ$_{25-35}$-induced decline in NDUFS3 protein level ($n = 3$). **j** qPCR assay result revealed that *ERβ siRNA* deprived PTA (20 μM) of its antagonistic capability against the o-Aβ$_{25-35}$ (20 μM)-induced decrease in Catalase ($n = 3$). All assays were performed in primary neurons. $^{\#}P < 0.05$, $^{\#\#}P < 0.01$, $^{\#\#\#}P < 0.001$ vs DMSO, $^{*}P < 0.05$, $^{**}P < 0.01$ and $^{***}P < 0.001$ vs o-Aβ$_{25-35}$, ns represented no significant, one-way ANOVA followed by Bonferroni's multiple comparisons test. Scale bar: 250 μm, 100 μm.

promoter of BDNF in primary neurons but had no binding affinities to Catalase in primary neurons or TLR4 in primary microglia.

PTA ameliorated cognitive dysfunction in APP/PS1 mice

To investigate the potential of PTA in ameliorating memory impairment of female APP/PS1 transgenic mice, MWM, and Y-maze mice behavioral assay were performed according to the published approaches [33, 63, 64].

MWM test. In 7-day training trails, the escape latencies to find the platform for APP/PS1 mice were obviously longer than those for WT mice, and administration of PTA (20, 40 $mg \cdot kg^{-1} \cdot d^{-1}$) efficiently ameliorated these prolongations of APP/PS1 mice (Fig. 5a and Supplementary Fig. S3a).

Y-maze test. The spontaneous alternation behavior of APP/PS1 mice was expectedly poorer than that of WT mice, and PTA administration (40 $mg \cdot kg^{-1} \cdot d^{-1}$) obviously improved the spontaneous alternation behavior of APP/PS1 mice (Fig. 5b and Supplementary Fig. S3b).

Therefore, all results indicated that PTA alleviated learning and memory impairment in APP/PS1 mice.

PTA treatment ameliorated Aβ pathology in brains of APP/PS1 mice

PTA reduced Aβ plaque load. As Aβ-induced senile plaque in the brain is a key neuropathology of AD, we investigated the potential suppression of PTA on Aβ deposition in brain of APP/PS1 mice by thioflavin S staining assay.

In the assay, the plaques were stained in green fluorescence. As indicated in Supplementary Fig. S2c, d, the plaque in either cortex or hippocampus of APP/PS1 mice was expectedly bigger than that of WT mice. Notably, PTA treatment (20, 40 $mg \cdot kg^{-1} \cdot d^{-1}$) efficiently reduced both senile plaque number and the average plaque-occupied area in the hippocampus and cortex of APP/PS1 mice (Fig. 5c–e and Supplementary Fig. S3c–f).

PTA treatment promoted microglial phagocytosis of Aβ via TLR4 upregulation in APP/PS1 mice. By considering that Iba1 as a specific marker of activated microglia could be used to characterize gliosis caused by oxidative stress and other reasons [65], Iba1 related assay was here performed to detect the recruitment of activated microglia to amyloid plaques in APP/PS1 mice by co-staining with Aβ [33].

In the assay, the colocalization rate of Aβ with Iba1 was quantified to evaluate the activity of PTA administration (20, 40 $mg \cdot kg^{-1} \cdot d^{-1}$) in promoting microglial phagocytosis of Aβ in APP/PS1 mice. The results shown that PTA administration efficiently promoted the recruitment of Iba1 positive cells to amyloid plaques in the hippocampus and cortex of APP/PS1 mice (Fig. 5f, g, and Supplementary Fig. S3g, h).

Next, qPCR and Western blot assays were performed to detect the regulation of PTA against TLR4 in the hippocampus and cortex of APP/PS1 mice, and the results (Fig. 5h–j and Supplementary Fig. S3i–k) demonstrated that PTA administration effectively promoted TLR4 level.

PTA treatment enhanced synaptic integrity in brains of APP/PS1 mice

PTA treatment upregulated dendritic spine integrity. Given that we have confirmed the capability of PTA in ameliorating synaptic damage by promoting the expression levels of synaptic integrity related proteins VAMP2 and PSD95 in neurons, we next investigated such beneficial effects of PTA in brains of APP/PS1 mice.

As expected, both immunofluorescence (Fig. 6a–d and Supplementary Fig. S4a–d) and Western blot (Fig. 6e, f, and Supplementary Fig. S4e, f) assay results implied that the densities and protein expression of VAMP2 and PSD95 were efficiently increased in the hippocampus and cortex of the PTA (20, 40 $mg \cdot kg^{-1} \cdot d^{-1}$)-treated APP/PS1 mice compared to those of the vehicle-treated APP/PS1 mice.

As indicated in the published reports, dendritic spines are the central sites of postsynaptic transmission and formation and elimination of spines is a lifelong dynamic process that is dependent on varied extra and intra-neuronal signals [66]. In addition, the shape and number of dendritic spines are closely related to the cognitive function [67, 68]. With these facts, we used Golgi staining [69] to investigate the integrity of dendrites and the number of dendritic spines of neurons in brains of the mice.

The results indicated that PTA administration (20, 40 $mg \cdot kg^{-1} \cdot d^{-1}$) obviously increased the development of the dendritic spine in the hippocampus and cortex of APP/PS1 mice (Fig. 6g and Supplementary Fig. S4g).

In addition, by considering that the hippocampal CA1 region functions potently in cognition [70], the spine density of the hippocampal CA1 region was also detected. The spine density in vehicle-treated APP/PS1 group was 0.71 ± 0.02 horns/μm, and such a value was obviously increased in PTA-treated mice (20 $mg \cdot kg^{-1} \cdot d^{-1}$, 1.28 ± 0.08 horns/μm; 40 $mg \cdot kg^{-1} \cdot d^{-1}$, 1.44 ± 0.11 horns/μm) (Fig. 6h, i).

Together, all data suggested that PTA protected synaptic integrity involving upregulation of dendritic spine integrity in APP/PS1 mice.

PTA ameliorated synaptic damage in brains of APP/PS1 mice via BDNF/TrkB/CREB pathway. Next, we also investigated the effect of PTA treatment on BDNF/TrkB/CREB signaling pathway in the hippocampus and cortex of the mice. Obviously, immunofluorescence and qPCR assay results revealed the increase of BDNF expression (Fig. 6j–l and Supplementary Fig. S4h–j), and Western blot results showed the upregulation of protein levels of BDNF, p-TrkB (Tyr 705) and p-CREB (Ser133) (Fig. 6m, n, and Supplementary Fig. S4k, l) in the hippocampus and cortex of PTA (20, 40 $mg \cdot kg^{-1} \cdot d^{-1}$)-treated APP/PS1 mice compared with those of vehicle-treated APP/PS1 mice.

Taken together, all results indicated that PTA ameliorated synaptic damage by regulation of BDNF/TrkB/CREB signaling pathway in APP/PS1 mice.

PTA treatment suppressed oxidative stress by regulating Catalase expression in APP/PS1 mice

Astrocyte is an abundant glial cell and a target cell of estrogen in the central nervous system (CNS) [71, 72]. It plays a more crucial role in regulating oxidative stress in CNS in comparison to neurons. In addition, GFAP-marked reactive astrogliosis is accepted as a universal marker of AD [73], and GFAP expression level in 6-month-old APP/PS1 mice was higher than in wild-type mice [74–77].

With these facts, immunofluorescence assay was performed to investigate the regulation of PTA treatment against the activation of astrocytes in the hippocampus and cortex of APP/PS1 mice by detecting GFAP expression level. The results indicated that PTA treatment (20, 40 $mg \cdot kg^{-1} \cdot d^{-1}$) obviously inhibited GFAP levels in the hippocampus and cortex of APP/PS1 mice (Fig. 7a, b, and Supplementary Fig. S5a, b). These results thus demonstrated that PTA treatment suppressed the activation of astrocytes.

In addition, MDA assay kit [78] was also used to investigate the regulation of PTA treatment against oxidative stress in the cortex of APP/PS1 mice. The results demonstrated that PTA treatment (20, 40 $mg \cdot kg^{-1} \cdot d^{-1}$) reduced MDA level (Supplementary Fig. S5c), indicative of the PTA treatment-induced suppression of oxidative stress.

Given that ERβ/Catalase pathway has been confirmed to be responsible for PTA-mediated suppression against oxidative stress

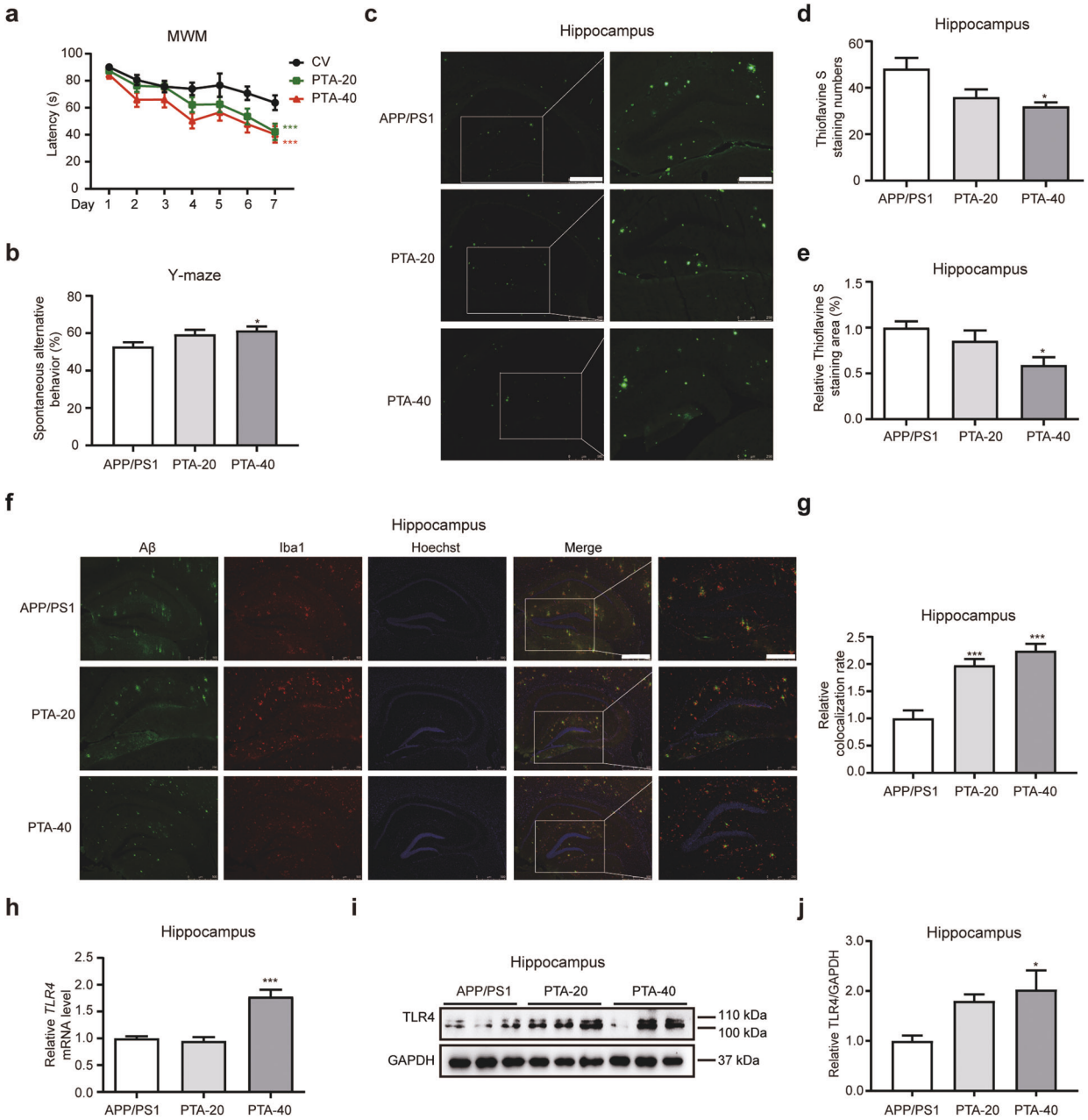

Fig. 5 PTA improved cognitive impairment and promoted microglial phagocytosis of Aβ in the hippocampus of APP/PS1 mice. a Results of escape latency during platform trials indicated that PTA treatment ameliorated the cognitive defect in APP/PS1 mice. $^{***}P < 0.001$ vs APP/PS1 group. Two-way ANOVA followed by Bonferroni's multiple comparisons test, $n = 12$. **b** Results of percentage of correct spontaneous alternation demonstrated that PTA treatment enhanced the spatial working memory defect in APP/PS1 mice ($n = 12$). **c**–**e** Micrographs of thioflavin-S staining and quantification results indicated that PTA decreased senile plaques in the hippocampus of APP/PS1 mice ($n \geq 3$). **f**, **g** Immunofluorescence assay with quantification results demonstrated that PTA increased the colocalization rate of Aβ and Iba1 in the hippocampus of APP/PS1 mice ($n = 5$). **h**–**j** qPCR and Western blot assays with qualification results demonstrated that PTA increased TLR4 expression in the hippocampus of APP/PS1 mice ($n \geq 3$). $^{*}P < 0.05$ and $^{***}P < 0.001$ vs APP/PS1 group. One-way ANOVA followed by Bonferroni's multiple comparisons test. Scale bar: 500 μm, 250 μm. APP/PS1: APP/PS1 mice treated with vehicle, PTA-20: APP/PS1 mice treated with PTA ($20\ mg \cdot kg^{-1} \cdot d^{-1}$), PTA-40: APP/PS1 mice treated with PTA ($40\ mg \cdot kg^{-1} \cdot d^{-1}$).

in neurons (Fig. 4f–j), we investigated the regulation of Catalase expression by PTA treatment in the hippocampus and cortex of APP/PS1 mice by qPCR assay. As expected, PTA treatment (20, 40 $mg \cdot kg^{-1} \cdot d^{-1}$) efficiently upregulated mRNA levels of Catalase (Fig. 7c, and Supplementary Fig. S5d).

Together, all results indicated that PTA decreased oxidative stress via upregulation of Catalase signaling in brains of APP/PS1 mice.

PTA suppressed apoptosis by regulation of Bcl-2 family proteins in APP/PS1 mice

According to the published reports, apoptosis is caused by a variety of reasons playing an important role in maintaining the homeostasis of the body, and tightly implicated in the pathology of AD [79], while Bcl-2 family functions potently in multiple pathways of apoptosis [80, 81]. With these facts, we investigated the potential effects of PTA treatment on the regulation of Bcl-2

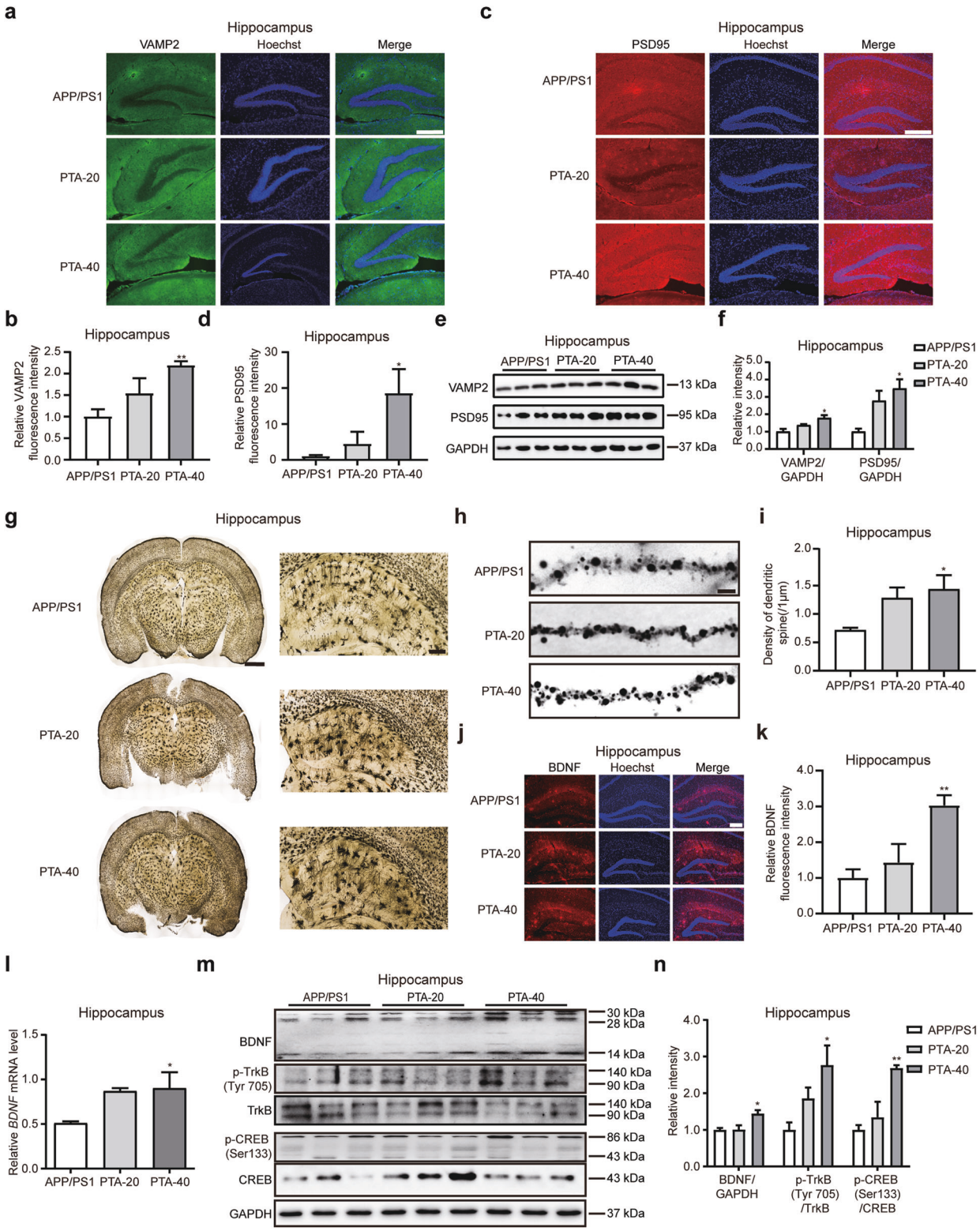

Fig. 6 PTA improved synaptic impairment and upregulated BDNF/TrkB/CREB pathway in the hippocampus of APP/PS1 mice. a–d Micrographs and quantification results demonstrated that PTA increased (**a**, **b**) VAMP2 and (**c**, **d**) PSD95 expressions in the hippocampus of APP/PS1 mice. $n = 5$. Scale bar: 250 μm. **e**, **f** Western blot assay with quantification results revealed that PTA increased VAMP2 and PSD95 expressions in the hippocampus of APP/PS1 mice ($n = 3$). **g–i** Golgi staining of dendritic spine with quantification results indicated that PTA treatment improved the spine density in the hippocampus of APP/PS1 mice. $n = 5$. Scale bar: 1000, 50, 5 μm. **j**, **k** Immunofluorescence and (**l**) qPCR assays with quantification results demonstrated that PTA increased BDNF expression in the hippocampus of APP/PS1 mice. $n \geq 4$. Scale bar: 250 μm. **m**, **n** Western blot assay with quantification results demonstrated that PTA upregulated the protein levels of BDNF, p-TrkB (Tyr 705) and p-CREB (Ser133) in the hippocampus of APP/PS1 mice ($n = 3$). $^{*}P < 0.05$ and $^{**}P < 0.01$ vs APP/PS1 group. One-way ANOVA followed by Bonferroni's multiple comparisons test. APP/PS1: APP/PS1 mice administrated with vehicle, PTA-20: APP/PS1 mice administrated with PTA ($20\ mg \cdot kg^{-1} \cdot d^{-1}$), PTA-40: APP/PS1 mice administrated with PTA ($40\ mg \cdot kg^{-1} \cdot d^{-1}$).

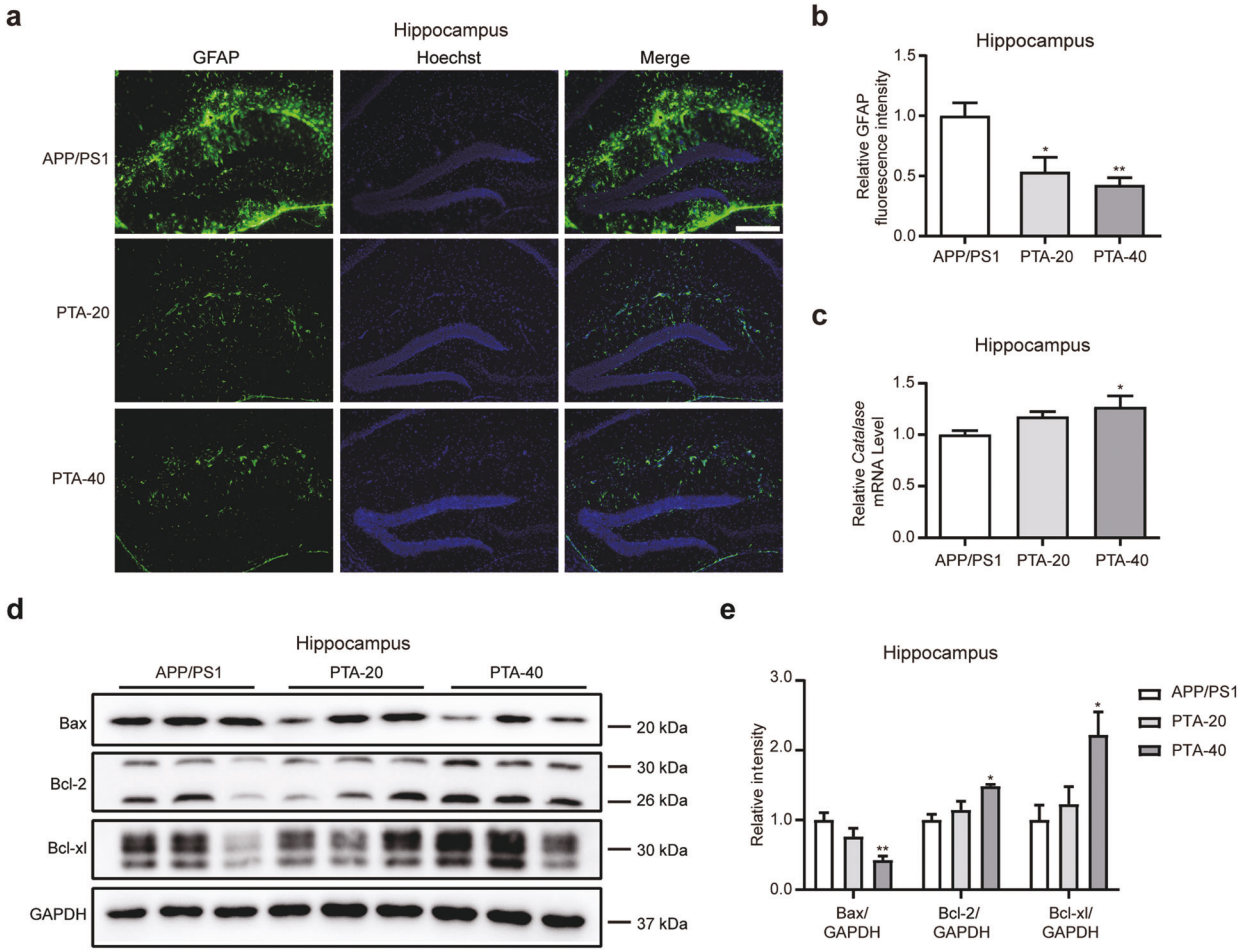

Fig. 7 PTA decreased oxidative stress and regulated Bcl-2 family proteins in the hippocampus APP/PS1 mice. a, **b** Immunofluorescence assay with quantification results demonstrated that PTA decreased GFAP expression in the hippocampus of APP/PS1 mice. $n = 5$. Scale bar: 250 μm. **c** qPCR assay results indicated that PTA improved Catalase expression in the hippocampus of APP/PS1 mice ($n = 4$). **d**, **e** Western blot with quantification results suggested that PTA regulated Bcl-2 family proteins expression in the hippocampus of APP/PS1 mice ($n = 3$). $^{*}P < 0.05$ and $^{**}P < 0.01$ vs APP/PS1 group. One-way ANOVA followed by Bonferroni's multiple comparisons test. APP/PS1: APP/PS1 mice treated with vehicle, PTA-20: APP/PS1 mice treated with PTA ($20\ mg \cdot kg^{-1} \cdot d^{-1}$), PTA-40: APP/PS1 mice treated with PTA ($40\ mg \cdot kg^{-1} \cdot d^{-1}$).

family proteins by Western blot assay in the hippocampus and cortex of APP/PS1 mice.

Western blot results showed that the level of pro-apoptotic protein Bax was significantly decreased and the levels of anti-apoptotic proteins Bcl-2 and Bcl-xl were increased in PTA-treated APP/PS1 mice (Fig. 7d, e, and Supplementary Fig. S5e, f).

DISCUSSION

Accumulating evidence has confirmed that brain estrogen deficiency is highly implicated in AD pathology [82–86], and estrogen therapy has been believed to be efficient in improving the dysfunction of cognition and reducing the risk of developing AD for postmenopausal women [87, 88]. Here, we also found that the estrogen level in brain of APP/PS1 mice was lower than that in WT mice, while the estrogen level in brain of 9-month-old APP/PS1 mice was lower than that in 6-month-old APP/PS1 mice (Spplementary Fig. S7), which is in accordance with the clinical data that estrogen level is downregulated in AD female patients and gradually declined with age [89]. Our results have thus provided the potential that 6-month-old APP/PS1 female mice might be suitable models for analysis of estrogen alternative therapy on AD.

ERβ selective agonist has been valued as a drug capable of avoiding the induction of the cancers of breast and other reproductive organs [90–93]. We determined that the natural product PTA as a selective ERβ agonist effectively alleviated AD-like pathology in female 6-month-old APP/PS1 mice, and the underlying mechanism has been intensively investigated. Our findings have provided new evidence for the role of ERβ in AD.

It was reported that hydroxytyrosol acetate improved the cognitive function of APP/PS1 transgenic mice in an ERβ-dependent manner and rendered no effects on Aβ accumulation and plaque formation [21]. In the current work, we determined that PTA enhanced microglial phagocytosis of o-$A\beta_{42}$ by promoting TLR4 expression, which is consistent with the result that estrogen treatment reduced Aβ accumulation and plaque formation [82, 94]. To our knowledge, our work has firstly reported the linkage of TLR4 to ERβ-mediated microglial phagocytosis of Aβ.

Synaptic plasticity impairment and synaptic loss in the brain are primary features of AD pathology and tightly related to AD progression [50, 95, 96], while Aβ-induced amyloid plaques and hyperphosphorylated Tau-composed neurofibrillary tangles are two major factors of synaptic disturbance [97–99]. As an ERβ selective agonist, PTA ameliorated synaptic deficit by reversing the declines of VAMP2 and PSD95 proteins through ERβ/BDNF/TrkB/CREB pathway. Moreover, we reported that ERβ increased BDNF transcription through binding to the promotor of BDNF. Our work might help better understand the role of ERβ in regulation of neuronal synaptic plasticity.

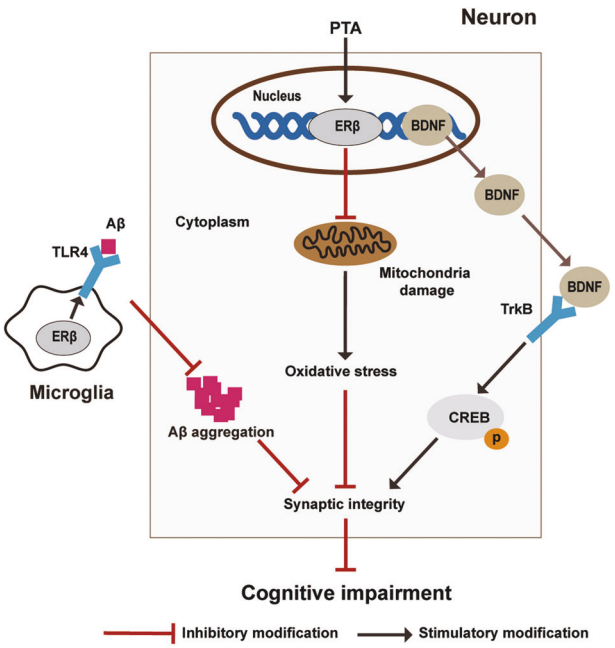

Fig. 8 Proposed mechanism for PTA in the amelioration of cognitive impairment of female APP/PS1 mice. PTA as an ERβ agonist efficiently improved the learning and memory impairments in female APP/PS1 mice. PTA reduced amyloid plaque deposition by promoting microglial o-Aβ_{42} phagocytosis through ERβ/TLR4 signaling. Meanwhile, PTA improved synaptic integrity through BDNF/TrkB/CREB signaling and ameliorated oxidative stress by increasing Catalase level.

Mitochondrial dysfunction is closely associated with AD [100]. It has been reported that ERβ agonism improved mitochondrial function in AD patients [101] and some small molecular agents regulated mitochondrial dysfunction by directly binding to ERβ on mitochondria [102]. In our work, we also extracted mitochondrial proteins from cytoplasmic proteins in response to PTA treatment, and Western blot results demonstrated that PTA had no impacts on ERβ level (Spplementary Fig. S2b, c). Our results implied that PTA improved mitochondrial function of neuronal cells through regulation of intracellular ERβ-mediated signaling cascades in nuclear instead of the influence on the expression of ERβ in mitochondria, and we determined that PTA reversed mitochondrial damage through ERβ/Catalase pathway. Thus, our work indicated that PTA could act as an antioxidant fighting against AD and other related neurodegenerative diseases.

Apoptotic neuronal cell death is an intuitive representation of AD [79] and Bcl-2 family proteins control apoptotic cell death in normal and abnormal cells [81]. It was noted that we determined the effect of PTA on Bcl-2 family proteins expression in APP/PS1 mice but failed to detect the regulation of PTA on Bcl-2 family protein in o-Aβ_{25-35}-treated neurons (data not shown). We tentatively suggested that such a PTA-induced in vivo effect was primarily due to the combined effects by the long-term treatment of PTA.

In AD pathology, it is believed that Aβ accumulation outside neurons of brains leads to varied harmful events including plaques formation, synaptic loss, oxidative stress, and neuronal apoptosis [103–105], while persistent oxidative stress aggravates the production and aggregation of Aβ and synaptic loss. Here, as summarized in the proposed schematic diagram (Fig. 8), PTA as a selective ERβ agonist reduced amyloid plaque deposition by promoting microglial o-Aβ_{42} phagocytosis through ERβ/TLR4 pathway. Meanwhile, PTA promoted synapse-related proteins VAMP2 and PSD95 via ERβ/BDNF/TrkB/CREB signaling and ameliorated oxidative stress through increasing Catalase expression. Therefore, all these combined beneficial effects of PTA contribute to the amelioration of PTA on cognitive impairment of AD model mice. Finally, our work has highly supported that selectively targeting ERβ is a promising therapeutic strategy for AD and highlighted the potential of PTA in the treatment of this disease.

ACKNOWLEDGEMENTS

This work was supported by Innovative Research Team of Six Talent Peaks Project in Jiangsu Province (TD-SWYY-013), the National Natural Science Foundation for Young Scientists of China (81703806), the Natural Science Foundation for Young Scientists of Nanjing University of Chinese Medicine (NZY81703806), the Open Project of Chinese Materia Medica First-Class Discipline of Nanjing University of Chinese Medicine (No. 2020YLXK018), and Postgraduate Research & Practice Innovation Program of Jiangsu Province (KYCX21_1737).

AUTHOR CONTRIBUTIONS

QYY, JYW, and XS designed the study. QYY, JLL, XYS, XNOY, and RFN performed the research. QYY and JLL wrote the paper. JL, YJH, and JZY contributed new reagents or analytic tools. QYY analyzed data. QYY, JLL, JYW, and XS are the guarantors of this work.

ADDITIONAL INFORMATION

Supplementary information The online version contains supplementary material available at https://doi.org/10.1038/s41401-021-00857-4.

Competing interests: The authors declare no competing interests.

REFERENCES

1. Nabavi SM, Talarek S, Listos J, Nabavi SF, Devi KP, Roberto de Oliveira M, et al. Phosphodiesterase inhibitors say NO to Alzheimer's disease. Food Chem Toxicol. 2019;134:110822.
2. Gjoneska E, Pfenning AR, Mathys H, Quon G, Kundaje A, Tsai LH, et al. Conserved epigenomic signals in mice and humans reveal immune basis of Alzheimer's disease. Nature. 2015;518:365–9.
3. Stoiljkovic M, Horvath TL, Hajos M. Therapy for Alzheimer's disease: missing targets and functional markers? Ageing Res Rev. 2021;68:101318.
4. Alzheimer's A. 2015 Alzheimer's disease facts and figures. Alzheimers Dement. 2015;11:332–84.
5. Irvine K, Laws KR, Gale TM, Kondel TK. Greater cognitive deterioration in women than men with Alzheimer's disease: a meta analysis. J Clin Exp Neuropsychol. 2012;34:989–98.
6. Wang JM, Irwin RW, Brinton RD. Activation of estrogen receptor α increases and estrogen receptor β decreases apolipoprotein E expression in hippocampus in vitro and in vivo. Proc Natl Acad Sci USA 2006;103:16983–88.
7. Lai YJ, Liu L, Hu XT, He L, Chen GJ. Estrogen modulates ubc9 expression and synaptic redistribution in the brain of APP/PS1 mice and cortical neurons. J Mol Neurosci. 2017;61:436–48.
8. Janicki SC, Park N, Cheng R, Lee JH, Schupf N, Clark LN. Estrogen receptor β variants modify risk for Alzheimer's disease in a multiethnic female cohort. J Alzheimers Dis. 2014;40:83–93.
9. Li J, Wang F, Ding H, Jin C, Chen J, Zhao Y, et al. Geniposide, the component of the Chinese herbal formula Tongluojiunao, protects amyloid-β peptide (1-42-mediated death of hippocampal neurons via the non-classical estrogen signaling pathway.Neural Regen Res.2014;9:474–80.
10. Li L, Xue Z, Chen L, Chen X, Wang H, Wang X. Puerarin suppression of Aβ_{1-42}-induced primary cortical neuron death is largely dependent on ERβ. Brain Res. 2017;1657:87–94.
11. Chhibber A, Zhao L. ERβ and ApoE isoforms interact to regulate BDNF-5-HT2A signaling and synaptic function in the female brain. Alzheimers Res Ther. 2017;9:79.
12. Lee S, Lee SO, Kim GL, Rhee DK. Estrogen receptor-β of microglia underlies sexual differentiation of neuronal protection via ginsenosides in mice brain. CNS Neurosci Ther. 2018;24:930–9.
13. Sohanaki H, Baluchnejadmojarad T, Nikbakht F, Roghani M. Pelargonidin improves memory deficit in amyloid β_{25-35} rat model of Alzheimer's disease by inhibition of glial activation, cholinesterase, and oxidative stress. Biomed Pharmacother. 2016;83:85–91.

14. Hidalgo-Lanussa O, Ávila-Rodriguez M, Baez-Jurado E, Zamudio J, Echeverria V, Garcia-Segura LM, et al. Tibolone reduces oxidative damage and inflammation in microglia stimulated with palmitic acid through mechanisms involving estrogen receptor β. Mol Neurobiol. 2017;55:5462–77.
15. Farkas I, Balint F, Farkas E, Vastagh C, Fekete C, Liposits Z. Estradiol increases glutamate and GABA neurotransmission into GnRH neurons via retrograde NO-signaling in proestrous mice during the positive estradiol feedback period. eNeuro 2018;5:e0057.
16. Pandey D, Banerjee S, Basu M, Mishra N. Memory enhancement by Tamoxifen on amyloidosis mouse model. Horm Behav. 2016;79:70–3.
17. Merlo S, Spampinato SF, Sortino MA. Estrogen and Alzheimer's disease: still an attractive topic despite disappointment from early clinical results. Eur J Pharmacol. 2017;817:51–8.
18. Chhibber A, Woody SK, Karim Rumi MA, Soares MJ, Zhao L. Estrogen receptor β deficiency impairs BDNF-5-HT_{2A} signaling in the hippocampus of female brain: A possible mechanism for menopausal depression. Psychoneuroendocrinology. 2017;82:107–16.
19. Jia M, Dahlman-Wright K, Gustafsson JA. Estrogen receptor α and β in health and disease. Best Pr Res. Clin Endocrinol Metab. 2015;29:557–68.
20. Petry FDS, Hoppe JB, Klein CP, Dos Santos BG, Hozer RM, Bifi F, et al. Genistein attenuates amyloid-β-induced cognitive impairment in rats by modulation of hippocampal synaptotoxicity and hyperphosphorylation of Tau. J Nutr Biochem. 2021;87:108525.
21. Qin C, Hu S, Zhang S, Zhao D, Wang Y, Li H, et al. Hydroxytyrosol acetate improves the cognitive function of APP/PS1 transgenic mice in ERβ-dependent manner. Mol Nutr Food Res. 2021;65:e2000797.
22. Hu G, Peng C, Xie X, Zhang S, Cao X. Availability, pharmaceutics, security, pharmacokinetics, and pharmacological activities of patchouli alcohol. Evid Based Complement Altern Med. 2017;2017:4850612.
23. Wang HT, Wang ZZ, Wang ZC, Wang SM, Cai XJ, Su GH, et al. Patchouli alcohol attenuates experimental atherosclerosis via inhibiting macrophage infiltration and its inflammatory responses. Biomed Pharmacother. 2016;83:930–35.
24. Liao JB, Wu DW, Peng SZ, Xie JH, Li YC, Su JY, et al. Immunomodulatory potential of patchouli alcohol isolated from Pogostemon cablin (Blanco) Benth (Lamiaceae) in mice. Trop Pharmacol Res. 2013;12:559–65.
25. Jeong JB, Shin YK, Lee SH. Anti-inflammatory activity of patchouli alcohol in RAW264.7 and HT-29 cells. Food Chem Toxicol. 2013;55:229–33.
26. Li YC, Xian YF, Ip SP, Su ZR, Su JY, He JJ, et al. Anti-inflammatory activity of patchouli alcohol isolated from Pogostemonis Herba in animal models. Fitoterapia. 2011;82:1295–301.
27. Jeong JB, Choi J, Lou Z, Jiang X, Lee SH. Patchouli alcohol, an essential oil of Pogostemon cablin, exhibits anti-tumorigenic activity in human colorectal cancer cells. Int Immunopharmacol. 2013;16:184–90.
28. Sah SP, Mathela CS, Chopra K. Antidepressant effect of Valeriana wallichii patchouli alcohol chemotype in mice: behavioural and biochemical evidence. J Ethnopharmacol. 2011;135:197–200.
29. Xu X, Lu Y, Chen L, Chen J, Luo X, Shen X. Identification of 15d-PGJ2 as an antagonist of farnesoid X receptor: molecular modeling with biological evaluation. Steroids. 2013;78:813–22.
30. Lu J, Zhang C, Lv J, Zhu X, Jiang X, Lu W, et al. Antiallergic drug desloratadine as a selective antagonist of 5HT2A receptor ameliorates pathology of Alzheimer's disease model mice by improving microglial dysfunction. Aging Cell. 2021;20:e13286.
31. Liu JF, Yan XD, Qi LS, Li L, Hu GY, Li P, et al. Ginsenoside Rd attenuates $Aβ_{25-35}$-induced oxidative stress and apoptosis in primary cultured hippocampal neurons. Chem Biol Interact. 2015;239:12–8.
32. Wang J, Yuan Y, Zhang P, Zhang H, Liu X, Zhang Y. Neohesperidin prevents $Aβ_{25-35}$-induced apoptosis in primary cultured hippocampal neurons by blocking the S-nitrosylation of protein-disulphide isomerase. Neurochem Res. 2018;43:1736–44.
33. Lv J, Wang W, Zhu X, Xu X, Yan Q, Lu J, et al. DW14006 as a direct AMPKα1 activator improves pathology of AD model mice by regulating microglial phagocytosis and neuroinflammation. Brain Behav Immun. 2020;90:55–69.
34. Welge V, Fiege O, Lewczuk P, Mollenhauer B, Esselmann H, Klafki HW, et al. Combined CSF tau, p-tau181 and amyloid-β 38/40/42 for diagnosing Alzheimer's disease. J Neural Transm (Vienna). 2009;116:203–12.
35. Holtzman DM, Morris JC, Goate AM. Alzheimer's disease: the challenge of the second century. Sci Transl Med. 2011;3:77sr1.
36. Zhao Y, Wu X, Li X, Jiang LL, Gui X, Liu Y, et al. TREM2 is a receptor for β-amyloid that mediates microglial function. Neuron. 2018;97:1023–31 e7.
37. Lian WW, Zhou W, Zhang BY, Jia H, Xu LJ, Liu AL, et al. DL0410 ameliorates cognitive disorder in SAMP8 mice by promoting mitochondrial dynamics and the NMDAR-CREB-BDNF pathway. Acta Pharmacol Sin. 2021;42:1055–68.
38. Lin SP, Wei JX, Hu JS, Bu JY, Zhu LD, Li Q, et al. Artemisinin improves neurocognitive deficits associated with sepsis by activating the AMPK axis in microglia. Acta Pharmacol Sin. 2021;42:1069–79.
39. Stine WB, Jungbauer L, Yu C, LaDu MJ. Preparing synthetic Aβ in different aggregation states. Methods Mol Biol. 2011;670:13–32.
40. Ito D, Imai Y, Ohsawa K, Nakajima K, Fukuuchi Y, Kohsaka S. Microglia-specific localisation of a novel calcium binding protein, Iba1. Mol Brain Res. 1998;57:1–9.
41. Jin X, Liu MY, Zhang DF, Zhong X, Du K, Qian P, et al. Baicalin mitigates cognitive impairment and protects neurons from microglia-mediated neuroinflammation via suppressing NLRP3 inflammasomes and TLR4/NF-κB signaling pathway. CNS Neurosci Ther. 2019;25:575–90.
42. Shi XZ, Wei X, Sha LZ, Xu Q. Comparison of β-amyloid plaque labeling methods: Antibody staining, gallyas silver staining, and Thioflavin-S staining. Chin Med Sci J. 2018;33:167–73.
43. Jerabek-Willemsen M, Wienken CJ, Braun D, Baaske P, Duhr S. Molecular interaction studies using microscale thermophoresis. Assay Drug Dev Technol. 2011;9:342–53.
44. Roher AE, Kokjohn TA, Clarke SG, Sierks MR, Maarouf CL, Serrano GE, et al. APP/Aβ structural diversity and Alzheimer's disease pathogenesis. Neurochem Int. 2017;110:1–13.
45. Gold M, El Khoury J. β-amyloid, microglia, and the inflammasome in Alzheimer's disease. Semin Immunopathol. 2015;37:607–11.
46. Li R, Shen Y, Yang L-B, Lue L-F, Finch C, Rogers J. Estrogen enhances uptake of amyloid. J Neurochem. 2000;75:1447–54.
47. Fujikura M, Iwahara N, Hisahara S, Kawamata J, Matsumura A, Yokokawa K, et al. CD14 and toll-like receptor 4 promote fbrillar Aβ42 uptake by microglia through a clathrin-mediated pathway. J Alzheimers Dis. 2019;68:323–37.
48. Jang SS, Chung HJ. Emerging link between Alzheimer's disease and homeostatic synaptic plasticity. Neural Plast. 2016;2016:7969272.
49. Hussain S, Davanger S. Postsynaptic VAMP/synaptobrevin facilitates differential vesicle trafficking of GluA1 and GluA2 AMPA receptor subunits. PLoS One. 2015;10:e0140868.
50. Skaper S, Facci L, Zusso M, Giusti P. Synaptic plasticity, dementia and Alzheimer disease. CNS Neurol Disord Drug Targets. 2017;16:220–33.
51. Wang S, Zhu J, Xu T. 17β-estradiol (E2) promotes growth and stability of new dendritic spines via estrogen receptor β pathway in intact mouse cortex. Brain Res Bull. 2018;137:241–8.
52. Galvin C, Ninan I. Regulation of the mouse medial prefrontal cortical synapses by endogenous estradiol. Neuropsychopharmacology. 2014;39:2086–94.
53. Bathina S, Das UN. Brain-derived neurotrophic factor and its clinical implications. Arch Med Sci. 2015;11:1164–78.
54. Meltser I, Tahera Y, Simpson E, Hultcrantz M, Charitidi K, Gustafsson JA, et al. Estrogen receptor β protects against acoustic trauma in mice. J Clin Invest. 2008;118:1563–70.
55. Kemper MF, Zhao Y, Duckles SP, Krause DN. Endogenous ovarian hormones affect mitochondrial efficiency in cerebral endothelium via distinct regulation of PGC-1 isoforms. J Cereb Blood Flow Metab. 2013;33:122–8.
56. Dixit S, Fessel JP, Harrison FE. Mitochondrial dysfunction in the APP/PSEN1 mouse model of Alzheimer's disease and a novel protective role for ascorbate. Free Radic Biol Med. 2017;112:515–23.
57. Varshney V, Garabadu D. Naringin exhibits mas receptor-mediated neuroprotection against amyloid β-induced cognitive deficits and mitochondrial toxicity in rat brain. Neurotox Res. 2021;39:1023–43.
58. Lin X, Wen X, Wei Z, Guo K, Shi F, Huang T, et al. Vitamin K2 protects against $Aβ_{42}$-induced neurotoxicity by activating autophagy and improving mitochondrial function in Drosophila. Neuroreport. 2021;32:431–7.
59. Wei X, Xu X, Chen Z, Liang T, Wen Q, Qin N, et al. Protective effects of 2-dodecyl-6-methoxycyclohexa-2,5 -diene-1,4-dione isolated from Averrhoa Carambola L. (Oxalidaceae) roots on neuron apoptosis and memory deficits in Alzheimer's disease. Cell Physiol Biochem. 2018;49:1064–73.
60. Caruso G, Spampinato SF, Cardaci V, Caraci F, Sortino MA, Merlo S. β-amyloid and oxidative stress: Perspectives in drug development. Curr Pharm Des. 2019;25:4771–81.
61. Long J, He P, Shen Y, Li R. New evidence of mitochondria dysfunction in the female Alzheimer's disease brain: deficiency of estrogen receptor-β. J Alzheimers Dis. 2012;30:545–58.
62. Henikoff S, Henikoff JG, Kaya-Okur HS, Ahmad K. Efficient chromatin accessibility mapping in situ by nucleosome-tethered tagmentation. eLife. 2020;9:e63274.
63. Turnbull MT, Boskovic Z, Coulson EJ. Acute down-regulation of BDNF signaling does not replicate exacerbated amyloid-β levels and cognitive impairment induced by cholinergic basal forebrain lesion. Front Mol Neurosci. 2018;11:51.
64. Qu X, Guan P, Han L, Wang Z, Huang X. Levistolide A attenuates Alzheimer's pathology through activation of the PPARγ pathway. Neurotherapeutics. 2020;18:326–39.

65. Khan A, Ikram M, Muhammad T, Park J, Kim MO. Caffeine modulates cadmium-induced oxidative stress, neuroinflammation, and cognitive impairments by regulating Nrf-2/HO-1 in vivo and in vitro. J Clin Med. 2019;8:680.
66. Koleske AJ. Molecular mechanisms of dendrite stability. Nat Rev Neurosci. 2013;14:536–50.
67. Gipson CD, Olive MF. Structural and functional plasticity of dendritic spines - root or result of behavior? Genes Brain Behav. 2017;16:101–17.
68. Sa-Nguanmoo P, Tanajak P, Kerdphoo S, Satjaritanun P, Wang X, Liang G, et al. FGF21 improves cognition by restored synaptic plasticity, dendritic spine density, brain mitochondrial function and cell apoptosis in obese-insulin resistant male rats. Horm Behav. 2016;85:86–95.
69. Zhao P, Qian X, Nie Y, Sun N, Wang Z, Wu J, et al. Neuropeptide S ameliorates cognitive impairment of APP/PS1 transgenic mice by promoting synaptic plasticity and reducing Aβ deposition. Front Behav Neurosci. 2019;13:138.
70. Sharifi F, Reisi P, Malek M. Synaptic plasticity in hippocampal CA1 neurons and learning behavior in acute kidney injury, and estradiol replacement in ovariectomized rats. BMC Neurosci. 2019;20:52.
71. Frost GR, Li YM. The role of astrocytes in amyloid production and Alzheimer's disease. Open Biol. 2017;7:170228.
72. Acaz-Fonseca E, Sanchez-Gonzalez R, Azcoitia I, Arevalo MA, Garcia-Segura LM. Role of astrocytes in the neuroprotective actions of 17β-estradiol and selective estrogen receptor modulators. Mol Cell Endocrinol. 2014;389:48–57.
73. Lassmann H, van Horssen J. Oxidative stress and its impact on neurons and glia in multiple sclerosis lesions. Biochim Biophys Acta. 2016;1862:506–10.
74. Tao CC, Cheng KM, Ma YL, Hsu WL, Chen YC, Fuh JL, et al. Galectin-3 promotes Aβ oligomerization and Aβ toxicity in a mouse model of Alzheimer's disease. Cell Death Differ. 2020;27:192–209.
75. Shi XM, Zhang H, Zhou ZJ, Ruan YY, Pang J, Zhang L, et al. Effects of safflower yellow on β-amyloid deposition and activation of astrocytes in the brain of APP/PS1 transgenic mice. Biomed Pharmacother. 2018;98:553–65.
76. Luo Y, Yang W, Li N, Yang X, Zhu B, Wang C, et al. Anodal transcranial direct current stimulation can improve spatial learning and memory and attenuate $A\beta_{42}$ burden at the early stage of Alzheimer's disease in APP/PS1 transgenic mice. Front Aging Neurosci. 2020;12:134.
77. Jorda A, Cauli O, Santonja JM, Aldasoro M, Aldasoro C, Obrador E, et al. Changes in chemokines and chemokine receptors expression in a mouse model of Alzheimer's disease. Int J Biol Sci. 2019;15:453–63.
78. Wan T, Wang Z, Luo Y, Zhang Y, He W, Mei Y, et al. FA-97, a new synthetic caffeic acid phenethyl ester derivative, protects against oxidative stress-mediated neuronal cell apoptosis and scopolamine-induced cognitive impairment by activating Nrf2/HO-1 signaling. Oxid Med Cell Longev. 2019;2019:8239642.
79. Obulesu M, Lakshmi MJ. Apoptosis in Alzheimer's disease: an understanding of the physiology, pathology and therapeutic avenues. Neurochem Res. 2014;39:2301–12.
80. Knight T, Luedtke D, Edwards H, Taub JW, Ge Y. A delicate balance - The BCL-2 family and its role in apoptosis, oncogenesis, and cancer therapeutics. Biochem Pharmacol. 2019;162:250–61.
81. Singh R, Letai A, Sarosiek K. Regulation of apoptosis in health and disease: the balancing act of BCL-2 family proteins. Nat Rev Mol Cell Biol. 2019;20:175–93.
82. Yue X, Lu M, Lancaster T, Cao P, Honda SI, Staufenbiel M, et al. Brain estrogen deficiency accelerates Aβ plaque formation in an Alzheimer's disease animal model. Proc Natl Acad Sci USA 2005;102:19198–203.
83. Ginsberg SD, Malek-Ahmadi MH, Alldred MJ, Chen Y, Chen K, Chao MV, et al. Brain-derived neurotrophic factor (BDNF) and TrkB hippocampal gene expression are putative predictors of neuritic plaque and neurofibrillary tangle pathology. Neurobiol Dis. 2019;132:104540.
84. Song JH, Yu JT, Tan L. Brain-derived neurotrophic factor in Alzheimer's disease: risk, mechanisms, and therapy. Mol Neurobiol. 2015;52:1477–93.
85. Choi SH, Bylykbashi E, Chatila ZK, Lee SW, Pulli B, Clemenson GD, et al. Combined adult neurogenesis and BDNF mimic exercise effects on cognition in an Alzheimer's mouse model. Science. 2018;361:eaan8821.
86. Liu S, Li X, Gao J, Liu Y, Shi J, Gong Q. Icariside II, a phosphodiesterase-5 inhibitor, attenuates β-amyloid-induced cognitive deficits via BDNF/TrkB/CREB signaling. Cell Physiol Biochem. 2018;49:985.
87. Tang M-X, Jacobs D, Stern Y, Marder K, Schofield P, Gurland B, et al. Effect of oestrogen during menopause on risk and age at onset of Alzheimer's disease. Lancet. 1996;348:429–32.
88. Simpkins JW, Yi KD, Yang SH, Dykens JA. Mitochondrial mechanisms of estrogen neuroprotection. Biochim Biophys Acta. 2010;1800:1113–20.
89. Li R, Cui J, Shen Y. Brain sex matters: estrogen in cognition and Alzheimer's disease. Mol Cell Endocrinol. 2014;389:13–21.
90. Beresford SAA, Weiss NS, Voigt LF, McKnight B. Risk of endometrial cancer in relation to use of oestrogen combined with cyclic progestagen therapy in postmenopausal women. Lancet. 1997;349:458–61.
91. Maggiolini M, Recchia AG, Bonofiglio D, Catalano S, Vivacqua A, Carpino A, et al. The red wine phenolics piceatannol and myricetin act as agonists for estrogen receptor α in human breast cancer cells. J Mol Endocrinol. 2005;35:269–81.
92. Hinsche O, Girgert R, Emons G, Gründker C. Estrogen receptor β selective agonists reduce invasiveness of triple-negative breast cancer cells. Int J Oncol. 2015;46:878–84.
93. Ramasamy K, Samayoa C, Krishnegowda N, Tekmal RR. Therapeutic use of estrogen receptor β agonists in prevention and treatment of endocrine therapy resistant breast cancers: observations from preclinical models. Prog Mol Biol Transl Sci. 2017;151:177–94.
94. Morinaga A, Hirohata M, Ono K, Yamada M. Estrogen has anti-amyloidogenic effects on Alzheimer's β-amyloid fibrils in vitro. Biochem Biophys Res Commun. 2007;359:697–702.
95. Yu J, Kwon H, Cho E, Jeon J, Kang RH, Youn K, et al. The effects of pinoresinol on cholinergic dysfunction-induced memory impairments and synaptic plasticity in mice. Food Chem Toxicol. 2019;125:376–82.
96. Kim J, Kim J, Huang Z, Goo N, Bae HJ, Jeong Y, et al. Theracurmin ameliorates cognitive dysfunctions in 5XFAD mice by improving synaptic function and mitigating oxidative stress. Biomol Ther (Seoul). 2019;27:327–35.
97. Collins JM, King AE, Woodhouse A, Kirkcaldie MT, Vickers JC. The effect of focal brain injury on β-amyloid plaque deposition, inflammation and synapses in the APP/PS1 mouse model of Alzheimer's disease. Exp Neurol. 2015;267:219–29.
98. Biundo F, Del Prete D, Zhang H, Arancio O, D'Adamio L. A role for tau in learning, memory and synaptic plasticity. Sci Rep. 2018;8:3184.
99. Singh B, Covelo A, Martell-Martinez H, Nanclares C, Sherman MA, Okematti E, et al. Tau is required for progressive synaptic and memory deficits in a transgenic mouse model of α-synucleinopathy. Acta Neuropathol. 2019;138:551–74.
100. Perez Ortiz JM, Swerdlow RH. Mitochondrial dysfunction in Alzheimer's disease: role in pathogenesis and novel therapeutic opportunities. Br J Pharmacol. 2019;176:3489–507.
101. Uddin MS, Rahman MM, Jakaria M, Rahman MS, Hossain MS, Islam A, et al. Estrogen signaling in Alzheimer's disease: molecular insights and therapeutic targets for Alzheimer's dementia. Mol Neurobiol. 2020;57:2654–70.
102. Sarkar S, Jun S, Simpkins JW. Estrogen amelioration of Aβ-induced defects in mitochondria is mediated by mitochondrial signaling pathway involving ERβ, AKAP and Drp1. Brain Res. 2015;1616:101–11.
103. Wu MN, Zhou LW, Wang ZJ, Han WN, Zhang J, Liu XJ, et al. Colivelin ameliorates amyloid β peptide-induced impairments in spatial memory, synaptic plasticity, and calcium homeostasis in rats. Hippocampus. 2015;25:363–72.
104. Ravi SK, Narasingappa RB, Prasad M, Javagal MR, Vincent B. Cassia tora prevents $A\beta_{1\text{-}42}$ aggregation, inhibits acetylcholinesterase activity and protects against $A\beta_{1\text{-}42}$-induced cell death and oxidative stress in human neuroblastoma cells. Pharmacol Rep. 2019;71:1151–9.
105. Ali MA, Menze ET, Tadros MG, Tolba MF. Caffeic acid phenethyl ester counteracts doxorubicin-induced chemobrain in Sprague-Dawley rats: Emphasis on the modulation of oxidative stress and neuroinflammation. Neuropharmacology. 2020;181:108334.